Università Degli Studi di Padova

Department of Industrial Engineering

Master Thesis in Energy Engineering

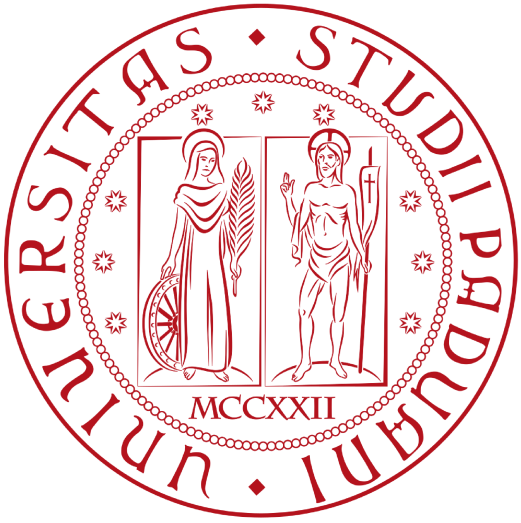

Optimisation of Battery and Electrolyzer size for a Wind-to-Hydrogen Plant

Master Candidate

Albarello Alessandro

Student ID 2020216

Supervisor

Prof. Anna Stoppato

Università Degli Studi di Padova

Co-supervisor

Dr. Paul Leahy

University College Cork

Academic Year 2022/2023

Do mo thaeghlach agus do mo chairde

To my family and friends

Contents

List of Figures

List of Tables

List of Acronyms

H2S Hydrogen System

ESS Energy Storage System

OS Optimisation System

NSGA-II Non Sorted Genetic Algorithm

CRITIC Criteria Importance though Intercrieria Correlation

TOPSIS Technique for Order Preference by Similarity to Ideal Solution

LCOH Levelized Cost of Hydrogen

EDP Energy Dump Possibility

PEM Polymer Electrolyte Membrane

WtHS Wind-to-Hydrogen System

WF Wind Farm

CS Control System

BSF Battery Size Factor

BL Baseload Level

OF Objective Function

EDP Energy Dump Possibility

BCR Benefit Cost Ratio

CAPEX CAPital EXpenditure

OPEX OPerational EXpenditure

DECEX DECommissioning EXpenditure

EPC Engineering Procurement and Construction

CC Controls and Communications

CLCOH Conversion LCOH

CCAPEX Conversion CAPEX

1

Introduction

The urge to tackle climate change, preventing the disastrous climatic events that are occurring more frequently all over the planet, combined with the necessity to move away from the dependency on fossil fuel resources, has led to a fast increase in the share of renewable energy in Europe, helped by increasingly ambitious policies promoted by the European Union.
The growth of renewables in the EU has been driven by the first Renewable Energy Directive (RED), that set a goal for all the member states to achieve at least a 16% share of renewables in their gross final energy consumption (GFC) by 2020. The EU reached, as an average value, a 21,8 % share of its gross final energy consumption from renewable sources in 2021, around 0,3% lower than in 2020, while in Ireland in 2020 it was 13,5%, therefore below the targets **[Fig.1.1] [Fig.1.2]** [17] [35].

From 2021, th RED directive has been followed by the second Renewable Energy Directive (REDII), setting a binding EU-target for a renewable share of 32% by 2030. In December 2018, Ireland submitted to the European Commission the National Energy & Climate Plan (NECP) 2021-2030 [10], containing the policies to deliver a 30% reduction by 2030 in non-ETS greenhouse gas emissions from 2005 levels, with the commitment of achieving an annual 7% reduction in GHG emissions. In 2019, the Climate Action Plan was approved (which was then followed by two amendments, in 2021 and 2023) to outline a pathway for 2030 that would reach the net zero emissions target by 2050 in accordance with the European Green deal and the Paris agreement [9]. In 2021, the European Commission updated the policies in terms of emissions reduction, by approving

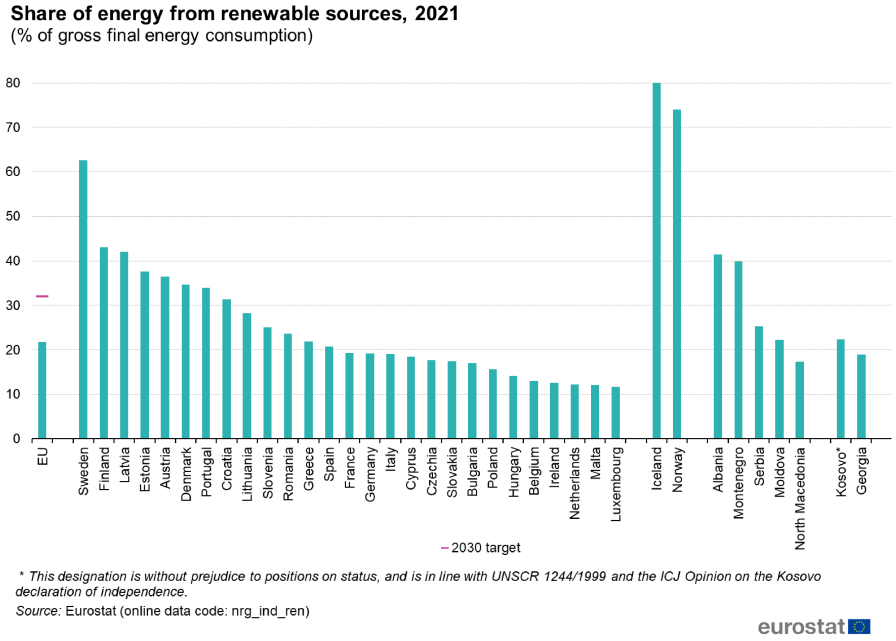

Figure 1.1: Share of energy from renewable sources in Europe in 2021

the Fit for 55 package, which set a binding obligation to the members of reducing the GHG emissions by at least 55% by 2030, increasing also the target from 32% to 40% of renewables into the energy mix [16]. In response to the Russian invasion of Ukraine in February 2022, in March 2022, another policy was approved, built on the implementation of Fit for 55, REPower EU, to phase out reliance on Russian gas, oil and coal, by enacting various measures, of which accelerating the development of renewables, and further developing the EU hydrogen market [15]. That considered, the Irish Climate Action Plan 2023 defined a roadmap to achieve the European targets, including a 75% emissions reduction in the energy sector, through phasing out coal and peat, and scaling up onshore wind capacity to 9 GW, solar to 8 GW, and offshore wind to 7 GW (with 2 GW dedicated to the production of green hydrogen) by 2030 [9] (the total installed wind capacity at 2021 accounted for 4339 MW **[Fig.1.3]** [34]).

Green hydrogen, produced through electrolysis using renewable sources, is expected to play an important role in the decarbonization process, by substituting hydrogen produced from fossil sources in the industry, but also as a new fuel and as a way to store excess power.

In the chemical industry, it is used mainly for the production of methanol (needed for the synthesis of heavier alcohols, gasoline, and other chemicals), and especially for ammonia, of which the total global production is used for

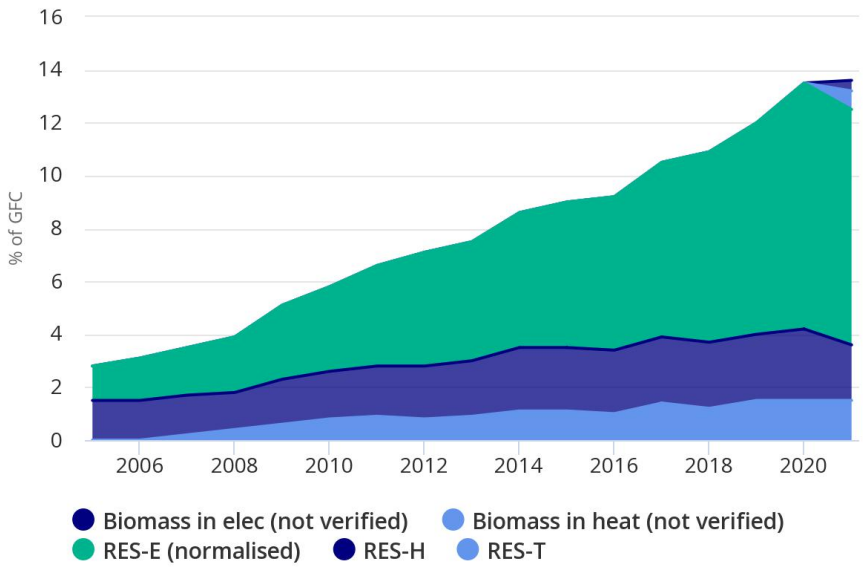

Figure 1.2: Overall Renewable Energy Share (RES) in Ireland

Growth of Renewable Energy Share in Ireland split into three modes, Electricity (E), Transport (T) and Heat (H).

more than 85% by fertiliser manufacturers [23]. Almost all the hydrogen for the synthesis of ammonia comes form steam methane reforming, which results in CO_2 emissions. Hydrogen is also used as a reducing agent in the Direct Reduction of Iron (DRI) for the steel production, and the substitution of the grey hydrogen (produced by the steam reforming of natural gas) with green hydrogen could help reduce carbon dioxide emissions, although it would not be possible to avoid them completely, as a source of carbon is still needed. Therefore, a CCUS (Carbon Capture Utilisation and Storage) unit would be necessary [23].

Green hydrogen could not only make a valuable contribution in the future by replacing grey hydrogen where it is already a part of the productive process, but it could be also integrated into other sectors that still rely on carbon-emitting fuels. For instance, it would be possible to inject it into the existing gas grid to reduce the the natural gas consumption, and it could be used in the transport sector, in Fuel Cell Electric Vehicles (FCEVs) as a complementary option to battery vehicles, specifically in the high duty segment (long-range or high utilisation rate vehicles, e.g. trucks, trains, buses, taxis, ferry boats, cruise ships, aviation, forklifts), were a full implementation of just batteries is currently unachievable [24]. Moreover, hydrogen could become a means of energy storage, even on a

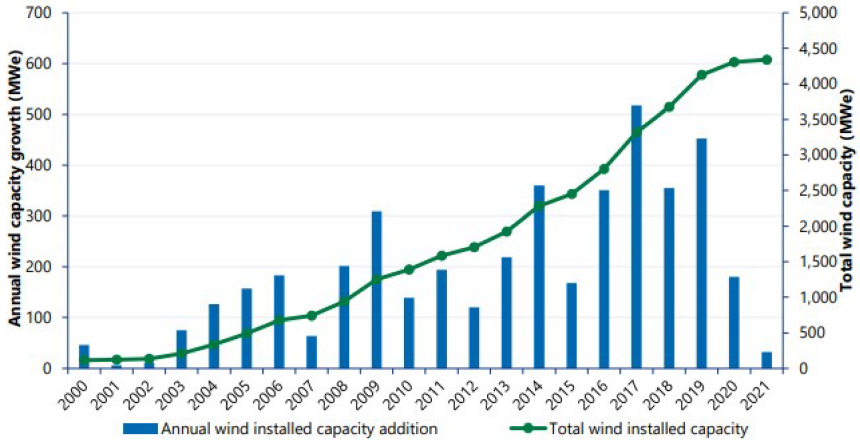

Figure 1.3: Annual and cumulative installed wind generating capacity from 2000 to 2022 in Ireland

seasonal basis, produced in areas with abundant renewable sources and then transferred over long distances to areas with scarce renewable resources, making the most of installed renewable energy capacity [24].

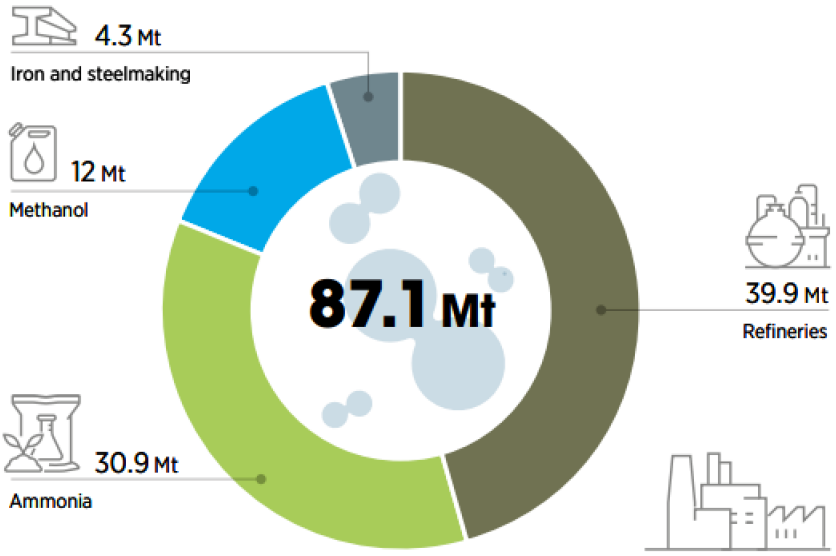

Figure 1.4: Pure global hydrogen demand in industry in 2020

Source: [23]

In 2021, the total global hydrogen production was 94 Mt, with an associated emission of 900 Mt_{CO_2}, almost entirely produced from fossil sources, with only 35 kt coming from electrolysis [21] **[Fig.1.5]**.

The International Energy Agency (IEA), estimates the production of hydro-

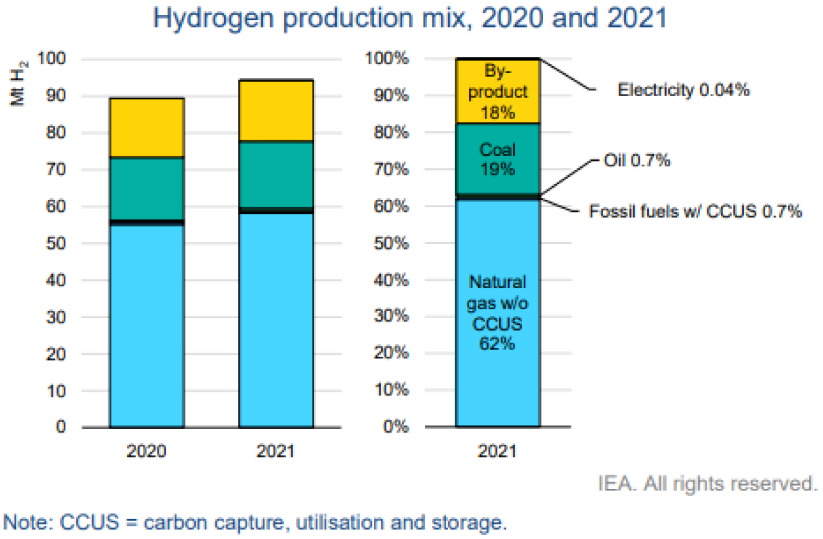

Figure 1.5: Hydrogen production mix in 2020 and 2021

gen through low-emission means (by electrolyzers and fossil fuels integrated with Carbon Capture Utilisation and Storage) to be more than 24 Mt by 2030, with Europe reaching close to 5 Mt [21].

In this regard, the H-Wind project (https://www.marei.ie/project/h-wind/), embedded in MaREI research centre in Cork, is contributing to establish a production chain in Ireland for green hydrogen, exploiting the abundant Irish offshore wind resources, as well as developing a new market for it, helping Ireland meeting the European and global targets for 2050.

This dissertation is the result of the work carried out within the H-Wind team, with the aim to determine the optimal sizing strategy for an offshore Hydrogen System (H2S) connected to an offshore Wind Farm (WF), investigating the possibility to include a Battery Energy Storage System (ESS) and analysing how different control strategies would work. An Optimisation System (OS) has been coded in Matlab to perform various simulations with different optimisation functions in various scenarios, to find an answer these questions.

2 Methodology

As stated in the Introduction, the goal of this project is to find an answer to these three main questions:

- **What is the optimal electrolyzer capacity of the Hydrogen System?**
- **Would an Energy Storage System be beneficial to it? And what would be its size?**
- **What is the best way to control the whole system?**

and to achieve this results, four main steps have been followed:

1. Defining the Preliminary Hypothesis
2. Gathering Information
3. Building the Optimisation System
4. Production and Analysis of the results.

2.1 Preliminary Hypothesis

The starting hypothesis used throughout the whole process, are presented here below:

- The system is hypothetically located off Kilmichael Point, which is situated in the South-East of Ireland, in the Irish Sea **[Figure 2.1]**.

Figure 2.1: Kilmichael Point location

- The energy source is the wind exploited by an off-shore wind park, and its size is 504 MW.
- It is supposed that all the turbines of the park produce the same power during every time step. The positioning of the turbines, the consequent losses and the different power production profiles are neglected, and the produced power is the one of the single reference turbine, multiplied by the number of the turbines of the park.
- The H2S and the ESS are located on an off-shore platform
- The technologies that have been modelled in the simulation are the Polymer Electrolyte Membrane (PEM) for the electrolyzers, and Lithium ions for the batteries (see discussion in Chapter 3).
- The production of hydrogen is the only purpose of the wind farm. All the generated power is sent only into the microgrid system, to produce hydrogen and to charge the ESS. The system is not hybrid (with competing production of hydrogen and electricity), and the exceeding power is dumped instead of being sent to the main grid.
- There is no storage system for the hydrogen, either onshore or offshore. As soon it is produced, it is sent into a pipeline that transports it into the mainland.

- It is supposed to build the system in 2030. Therefore, costs and the choice of the technologies should take 2030 as a reference.

The scheme of the offshore plant here hypothesised is shown in **[Figure 2.2]**.

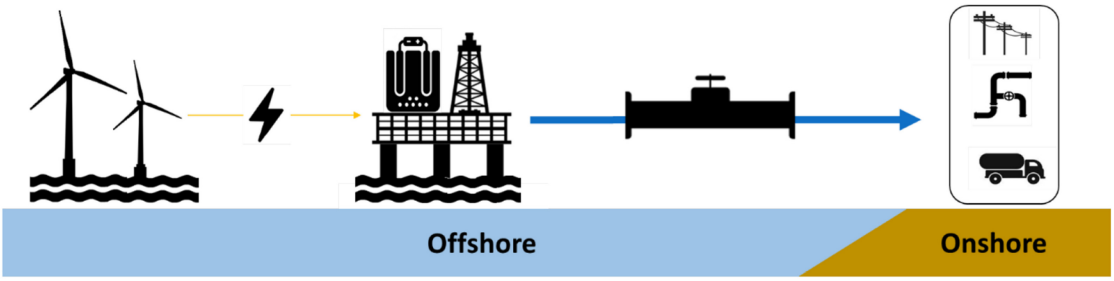

Figure 2.2: Schematising of the offshore plant.

Courtesy from [12]

2.2 Gathering Information

The goal of this preliminary phase, was to understand the problem and choose the possible solutions to solve it, by searching in the literature for any researches that have tackled similar design problems, as well as getting a better insight into the technologies here considered.
Tebibel [36] addressed a similar situation, for a small scale plant, by choosing the number of wind turbines, battery banks, electrolyzer stacks and hydrogen storage tanks, through a multiobjective algorithm optimising functions like the Levelized Cost of Hydrogen (LCOH), the Energy Dump Possibility (EDP), and others related to the CO_2 emissions and natural gas usage avoided. Atteme et al. [5] tried to minimise the costs while providing energy by mean of a single wind turbine, including a storage system composed of electrolyzers, fuel cells, battery banks and supercapacitors, sizing it adopting a genetic algorithm. Extremely relevant for this research have been the work of Xu et al. [41], where they adopted a set of algorithms, to find and rank the best sets of parameters, for the configuration of a Wind/PV park to feed an off-grid industrial load, using hydrogen as a mean of energy storage. All of them resemble in a certain way the hypothesis and the purposes of this project, but they differ for other aspects, especially for having a variable, instead of a fixed, wind power capacity, and for the need to fulfil the load's requirements or an hydrogen demand. Therefore their results have been adopted and adapted to match the characteristics specific

to this problem, especially in the structure of the control system and in the choice of the multiobjective functions.

2.3 Optimisation System

To the Optimisation System are given as input the performance parameters and the main working characteristics of the components (like number of turbines in the wind park, nominal power, efficiencies at nominal load, conversion efficiencies, lifetime of the project, etc), which are then used to run the models inside it. In addition, the OS is comprised of two main parts, the Physical component and the Decision component. The basic scheme of the OS is depicted in **[Fig.2.3]**.

2.3.1 Physical Component

The Physical component simulates the behaviour of the Wind-to-Hydrogen System (WtHS) for a given wind power profile used as input in the software. Its components, the electrolyzers and the batteries, have been coded in the software, and their operation is coordinated by a control system, that follows a given set of rules to improve the working conditions and usage of the system. For this study, two different control strategies have been adopted and compared, and are showed in Chapter 4.

2.3.2 Decision Component

The decision component is composed of three algorithms, that use the Physical component to find the best set of solutions to optimise the two decision variables (electrolyzer and battery size), by minimising some given objective functions, as it has been suggested by Xu et al. [41]. The first one to be used, is the Non Sorted Genetic Algorithm (NSGA-II), that by randomly generating and mutating populations (containing these decision variables) finds a set of Pareto points that minimise the selected objective functions. Then, to evaluate the Pareto front thus obtained, the CRITIC algorithm (Criteria Importance though Intercrieria Correlation) weights every solution, and finally the TOPSIS algorithm (Technique for Order Preference by Similarity to Ideal Solution) ranks

each of them from first to last. Each algorithm is described in detail in Chapter 6.

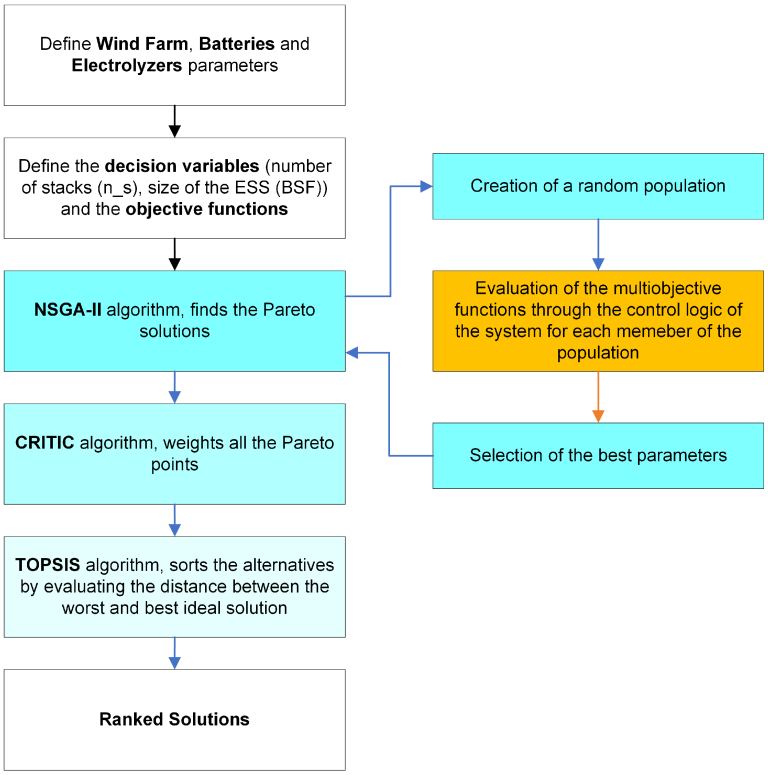

Figure 2.3: Schematising of the Optimisation System

The orange block represents the Physical component, the blue blocks the Decision components.

2.4 Simulation and Analysis

During the simulations, many different combinations of multiobjective functions are tried, in order to verify which choice allows to find the most convenient coupling solution. Also, the two different control schemes are compared to see the differences in their performances, and the same simulations are run again varying the efficiency profiles for the electrolyzers. Finally, all the results are put together and compared to draw the final conclusions.

3

System Components

The wind-to-hydrogen system is made of three main units, the wind farm, used to convert the energy from the wind into power, the hydrogen system, for the production of hydrogen through the electrolysis of water, and the energy storage system, used to store the surplus energy from the wind and to deliver it to the H2 system during low wind periods.

The layout of the system is that of a Centralised Offshore Electrolysis [20], where the power produced by the WF is sent to an offshore platform where the H2S and the ESS are located (together with other elements like the converter and rectifier, a cooling unit, a water desalinisation and a compression unit). The hydrogen produced by the electrolyzers is then transported to the mainland through a pipeline. This configuration simplifies the maintenance procedure making easier the access to the turbines than in a decentralised electrolysis system, and to the H2S and ESS, all located in the same offshore platform. On the other hand, it is more sensible to problems related to failure events not having any redundancies [20].
The power transmission from the WF is more advantageous via HVAC for a subsea transmission line with a length shorter than 60 km [20], that being the range for which the transmission losses and the costs are lower than HVDC (for a greater length, HVAC requires a greater section due to skin effect and self-induced reactance that increases the costs). The electrical layout, shown in **[Fig.3.1]**, has been derived from the islanded mode microgrid studied in [26], where the electrolyzers and the ESS are connected to an AC bus where they ex-

change power by means of a rectifier and a bidirectional converter. The electrical connections will not be discussed any further into this dissertation in order to keep the system simple and reasonably fast in terms of computations, by just considering the power exchanged by the components (instead of a dynamic behaviour of current and voltage). The power conversion units will be evaluated only in terms of their efficiency (taken as a constant, while in reality it would be function of the load) **[Tab.3.1]**.

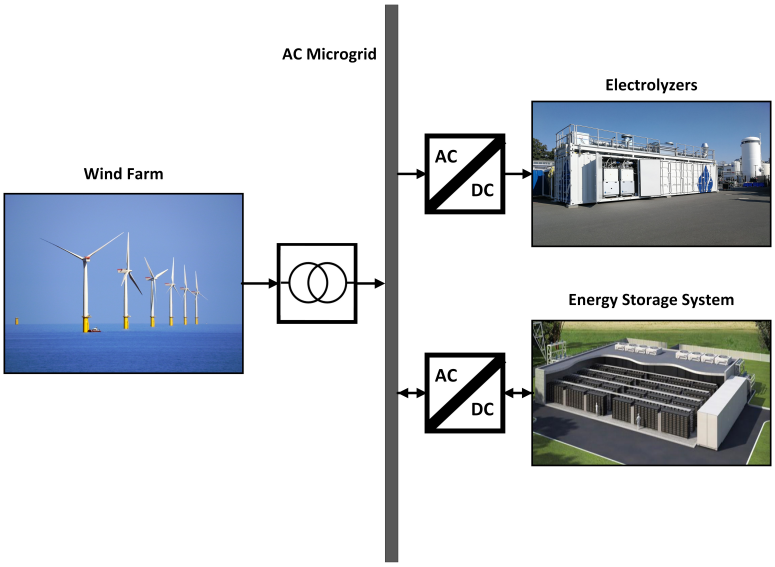

Figure 3.1: Electrical layout of the Wind-To-Hydrogen system

WF transformer $\eta_{transf,WF}$	94 %
ESS converter $\eta_{conv,Bat}$	95 % [36]
Electrolyzer rectifier $\eta_{DC,El}$	93% [13]

Table 3.1: Efficiencies of the power converter units

3.1 Wind Farm

According to the preliminary hypothesis formulated in Chapter 2, the wind farm has been modelled in a simplified way, starting from a single turbine, for which the yearly power profile is obtained, which is then multiplied by the overall number of turbines in the WF.
The wind data have been obtained from the website Renewable Ninja [32], that by selecting a location, the reference year, and the hub height, gives the wind

speed data for each hour time step. Then to find a suitable turbine, have been taken into consideration the wind power profiles contained inside the Offshore Wind Turbine Documentation by NREL, the National Renewable Energy Laboratory (https://nrel.github.io/turbine-models/Offshore.html), wich provides off-shore turbine descriptions of different sizes. The starting idea was to adopt a turbine with a size greater than 10 MW, as turbines greater than 10 MW will be installed in the coming five years, therefore both 12 MW and 15 MW turbines have been considered. As shown in Section 3.1.2, it was preferable to use a 12 MW turbine, as the transition between partial load to nominal power was smoother than for the 15 MW turbine power curve. Subsequently, the wind speed profile have been obtained in relation to the hub height of the chosen turbine, and it has been analysed to check if the turbine characteristics were compatible with the chosen site.

3.1.1 Wind Speed Profile

The hourly wind speed data of the 2019, obtained from Renewable Ninja website, come from the atmospheric dataset from NASA MERRA-2 (Modern-Era Retrospective analysis for Research and Applications, Version 2) [1]. They have been imported into Matlab where it was performed a preliminary analysis by obtaining the maximum, minimum and average value of the speed. These results are shown in **[Tab.3.2]**, **[Fig.3.2]** and **[Fig.3.3]**.

Max Wind Speed	23.6 m/s
Minimum Wind Speed	2.1 m/s
Yearly Average Wind Speed	9.5 m/s

Table 3.2: Maximum, minimum and average value of the wind speed in Kilmichael Point during 2019

The average wind speed values even though provides still useful information about the the location, it is not suitable for the sizing of the wind turbine that will be part of the offshore WF. Therefore, it is necessary to deepen the analysis, through the utilisation of the Weibull statistical distributions, defined in such way:

$$D(v) = \frac{k}{s} \cdot \left(\frac{v}{s}\right)^{k-1} exp\left[-\left(\frac{v}{s}\right)^{k}\right] \tag{3.1}$$

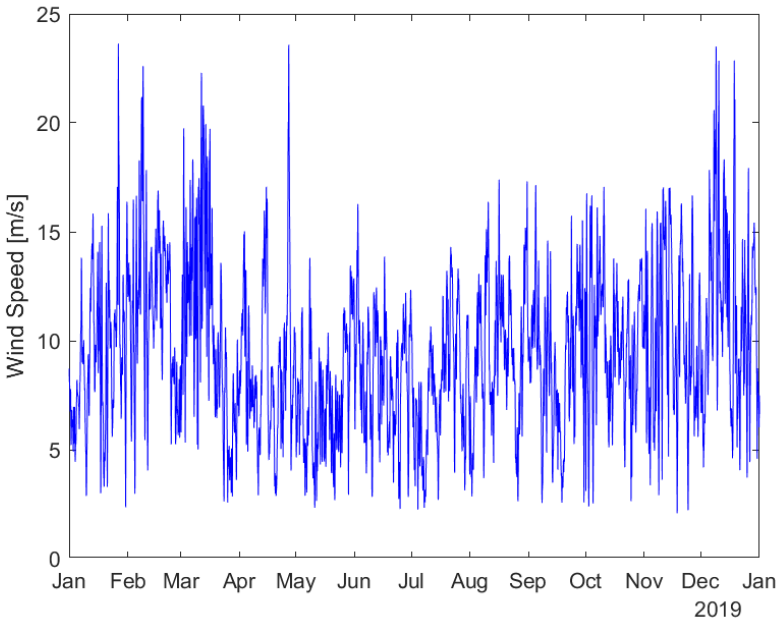

Figure 3.2: Wind speed profile of Kilmichael Point during 2019

$$C(v) = 1 - exp\left[-\left(\frac{v}{s}\right)^{k}\right] \tag{3.2}$$

where v is the wind speed, D the probability density function , C is the cumulative distribution function **[Fig.3.4]**, s the scale parameter and k the shape factor. In this case the parameters for the Weibull distributions that have been chosen are $k = 2.9$ and $s = 9$. Thanks to these, it is now possible to find two other parameters that are more interesting:

$$\hat{v} = s \cdot (ln2)^{\frac{1}{k}} \tag{3.3}$$

$$v_{maxE} = s \cdot \left(\frac{k+2}{k}\right)^{\frac{1}{k}} \tag{3.4}$$

with $\hat{v}$ that is the median speed, the velocity at which there is the 50% probability of having an higher speed and 50% of having it lower, and v_{maxE} which is the maximum available energy speed, the one that provides the maximum

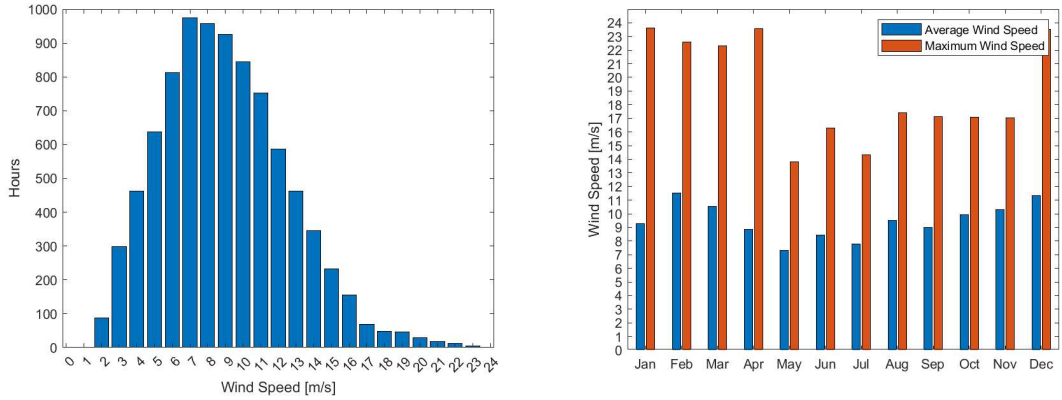

Figure 3.3: Wind speed distribution and monthly average and maximum values of the wind speed

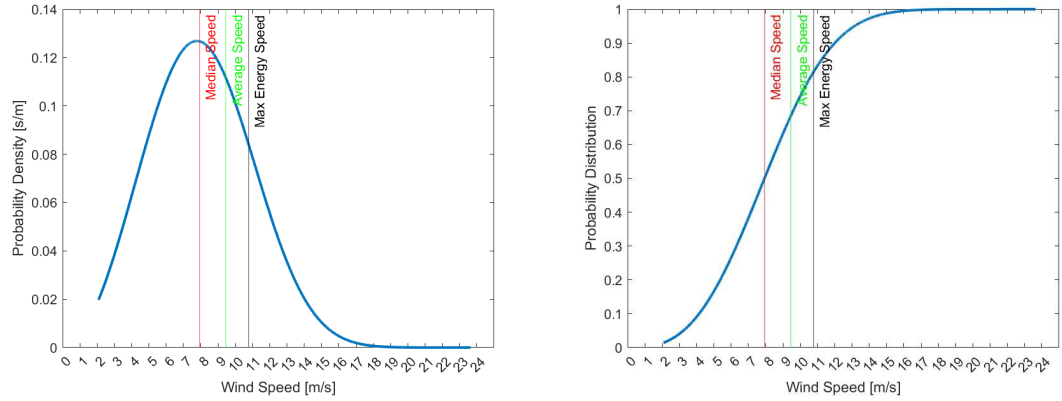

Figure 3.4: Probability density function and cumulative distribution function

contribution to energy availability. The values obtained are shown in **[Tab.3.3]**. Therefore 11 m/s appears to be a rated speed suitable for that location.

Median Wind Speed	7.9 m/s
Max Energy Wind Speed	10.8 m/s

Table 3.3: Median and maximum available energy speed

3.1.2 Wind Power Profile

The turbine that have been chosen is the *OR Cost Reference 12 MW* by NREL [29]. The power coefficient curve and the power profile have been obtained at https://nrel.github.io/turbine-models/2019ORCost_NREL_Reference_12MW_222.html, which have been then interpolated inside Matlab to be used to compute the power generation of the turbine.
As it can be seen, the power curve **[Fig.3.5]** shows a behaviour which is not completely realistic, due to the transition from the low wind speed condition to the nominal power condition, that does not happen smoothly. It has been interpolated with the points made available by NREL, and it was preferred to the 15 MW turbines, since in those, the transition was even more abrupt. Therefore, it has to be noticed that the energy production will be slightly overestimated. The values of the cut-in, cut-out and of the rated wind speed **[Tab.3.4]**, are compatible with the considerations drawn in Section 3.1.1, related to the wind characteristics and the maximum available energy speed.

Location Coordinates	52° 38′ 60″ N, 6° 0′ 0″ W
Rated Power P_{nom}	12000 kW
Rated Wind Speed v_{nom}	11 m/s
Cut-in Wind Speed v_{cut-in}	3 m/s
Cut-out Wind Speed $v_{cut-out}$	25 m/s
Rotor Diameter D_{rot}	222 m
Hub Height	136 m

Table 3.4: NREL 12 MW turbine characteristics

The power generated by the turbine during each time step t by the turbine, is then calculated as follows:

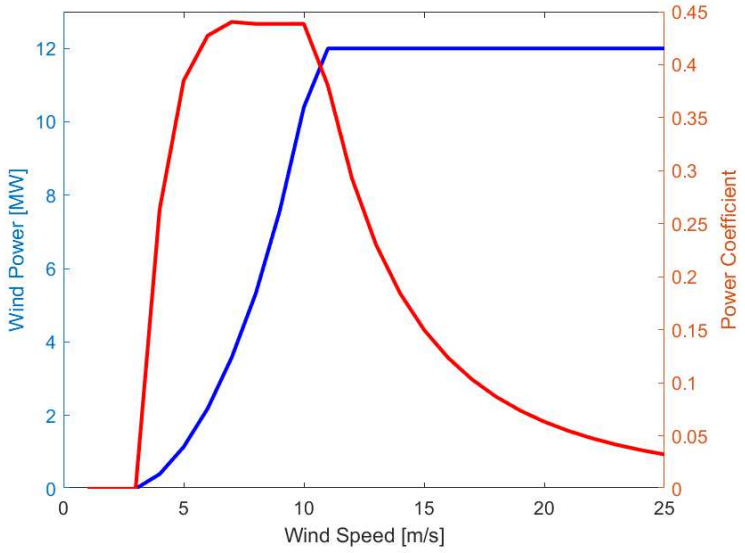

Figure 3.5: Power and Cp curves of the IEA 12 MW RWT turbine

$$P_{turbine}(t) = \begin{cases} 0 & v_{wind}(t) < v_{cut-in} \\ \frac{1}{2} \cdot \rho_{air} \cdot A \cdot C_p \cdot v_{wind}(t)^3 & v_{cut-in} \leq v_{wind}(t) < v_{nom} \\ P_{nom} & v_{nom} \leq v_{wind}(t) \leq v_{cut-out} \\ 0 & v_{wind}(t) > v_{cut-out} \end{cases} \tag{3.5}$$

where ρ_{air} is the density of the air, and it is taken as $1,225\, kg/m^3$, A is the rotor swept area and it is calculated as $A = \left(\pi \cdot D_{rot}^2\right)/4$, and C_p is the power coefficient.
The average capacity factor has been estimated as 49.7188 %, and in **[Fig.3.6]** can be seen the monthly variation.

Once power production profile from a single turbine has been obtained, the model of the whole wind farm is derived from it following the hypothesis of Chapter 2.1. It is supposed that every turbine produces power as the reference turbine $P_{turbine}$, the layout of the WF is neglected, and just the wake losses are

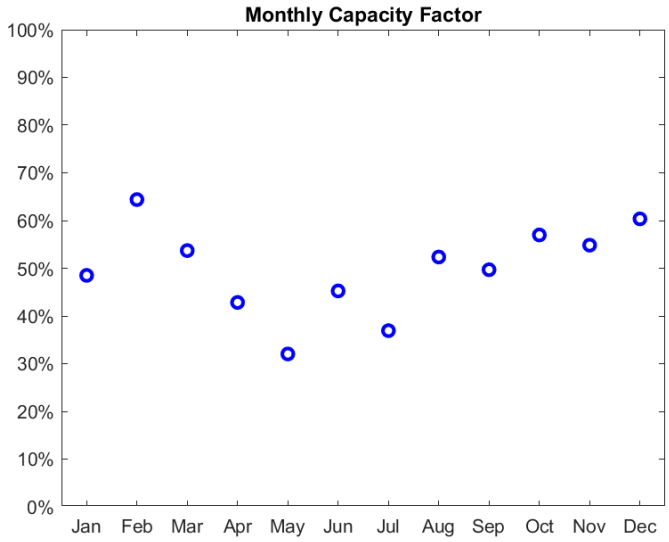

Figure 3.6: Monthly average capacity factor variation in the 12 MW turbine

considered and are taken as a constant. Considering the initial hypothesis of a 500 MW WF, and the size of the turbine $S_T = 12MW$, it is decided to have the WF composed of 42 turbines, for an overall capacity of the wind farm C_{WF} of 504 MW.
Thus, finally defined the wind farm, it is calculated the total power produced P_{WF} during each time step t, as:

$$P_{WF}(t) = n_T \cdot \eta_{Transf} \cdot (1 - w_{loss}) \cdot P_{turbine}(t) \tag{3.6}$$

while the total yearly energy production E_{WF} is:

$$E_{WF} = n_T \cdot \eta_{transf,WF} \cdot (1 - w_{loss}) \cdot \int_0^{8760} P_{turbine}(t) \cdot dt \tag{3.7}$$

where n_T is the number of turbines in the WF, $\eta_{transf,WF} = 94\,\%$ is the transformer efficiency and $w_{loss} = 10\,\%$ are the wake losses.
According to this methodology, the total energy production for the reference year 2019 of the modelled WF, has been estimated as 2.3213 TWh, and the maximum power production after losses and transformer is $426MW$. The energy yield monthly profile is shown in **[Fig.3.7]**.

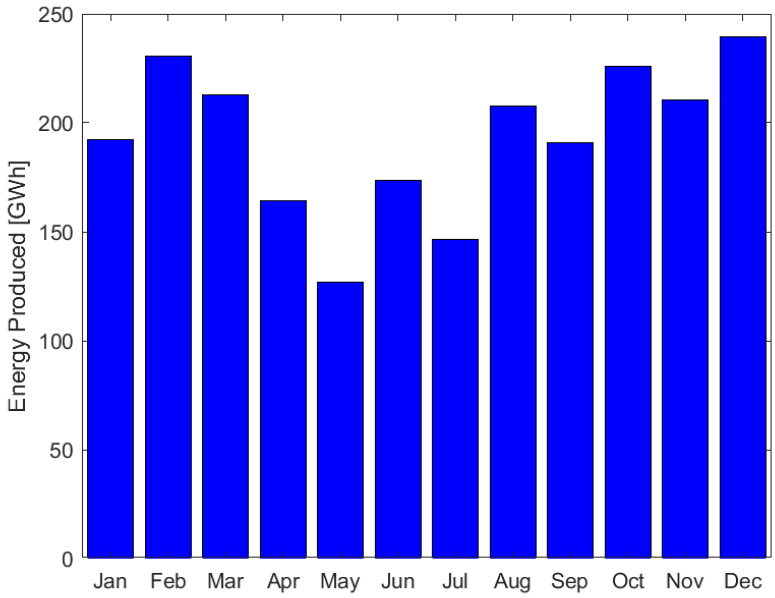

Figure 3.7: Monthly energy production profile of the Wind Farm

3.2 Electrolyzer

The electrolyzer is the central and most relevant component of the system, the one that produces hydrogen through the electrolysis of water, exploiting the power obtained from the energy of the wind, or the one deployed by energy storage devices.

There are three main technologies that are either currently widespread, or that are soon expected to be, alkaline, acidic, and solid oxide. This last one shows already noticeable advantages in term of efficiencies and it is foreseen to be one of the predominant technologies in the future, however, it is currently in in its research and development phase [3] [14] and therefore it won't be discussed here.

Before coding the electrolyzer model to implement in the optimisation system, it was necessary to decide between either Alkaline or PEM (Proton Exchange Membrane, part of the acidic electrolyzers). The main advantage of Alkaline technology is its maturity and commercial availability, and its reduced costs, given by the possibility of adopting cheap manganese and tungsten electrolytes, instead of more expensive and rare ones, like palladium (that are on the contrary necessary in PEM electrolyzers). On the other hand, its low efficiency and

low current density, require the stacks to be bigger when adopted in big scale system, increasing relevantly the overall cost. In addition to that, the hydrogen that produces, is less pure with respect to other technologies [3]. But the most problematic drawbacks lay in its low response to load variations and high minimum loads (15%-40%) acceptable for a correct operation, making them suitable for fixed load usages, but hardly matchable with fluctuating renewable sources [3]. In regards to PEM, even if the cost is higher (mainly due to its catalysts materials), its flexibility and its minimum operating load (5%-10%) [3], make it optimal for RES coupling. Furthermore, its easier maintenance makes it better choice when it has to be located in offshore platforms [7] [12]. Thus, for all the reasons above, the technology chosen is PEM over Alkaline (as anticipated in Section 2.1).

3.2.1 Modelling the electrolyzer

The first idea for this project was not to use Matlab, but instead, to build a very detailed model of an electrolyzer inside Simulink. Many models that are available in the literature, usually reach a considerable level of detail, evaluating the cell voltage and current, and its changing temperature profile. Frangiacomo et al. [18] developed an electrolyzer model composed of multiple submodels that simulated various interconnected domains (fluid dynamic, thermal, thermodynamic and electrochemical), and allowed to obtain the cell voltage and hydrogen output by giving the input current and the temperature. Ygit et al. [42] proposed a very detailed block scheme where anode, cathode and membrane where modelled, using the current and temperature as inputs as well. On the contrary, Möller et al. [28] built an hybrid system comprised of a PV plant, electrolyzer and battery, that did not require the cell temperature, but was able to calculate it through iterations. The main problem that arose when trying to build something similar, was the lack of certain inputs (especially the cell temperature), that made the whole model even more complex and full of loops. This was partially overcome by using and partially modified electrolyzer model built with Simscape blocks, available inside the Mathworks library (https://it.mathworks.com/help/simscape/ug/pem-electrolysis-system.html). Even though this provided good and very detailed results, it has proven itself extremely slow (to process just few tens of time steps it requires about 1/2 minutes), and considering that a simulation for a full year

is composed of 8760 time steps, and that inside the OS this is calculated for 200 different electrolyzers/battery combinations, and then repeated for 30 times (see Chapter 6), using such method would have required an excessive computation time. All this considered, it was then opted to develop a more simplistic model, by coding it into Matlab.

The detailed evaluations of the cell's temperature and voltage have been taken out, leading to a simpler way to estimate the hydrogen output, just by mean of the power input $P_{IN,El}$ from the WF and the ESS [37] [31] [14]:

$$H_2 = \frac{P_{IN,El} \cdot \eta_{electrolyzer} \cdot \eta_{DC,El}}{HHV} \tag{3.8}$$

where H_2 is the hydrogen generated in kg, $\eta_{electrolyzer}$ is the efficiency of the electrolyzer and HHV is the Higher Heating Value of hydrogen (39.41 kW/kg_{H_2}). The use of the HHV is preferred to the Lower Heating Value (LHV) when the hydrogen is regarded as a chemical product instead of being a mean of energy storage [31], and also because the enthalphy of evaporation has to be provided by the process [14].
Usually in the electrolyzers models, like in those described above, the efficiency is calculated after the hydrogen production has been found (it can be considered function of the cell voltage and temperature), while in other simplified models that use Equation (3.8), they consider it as a constant. In this situation, it was considered to be more convenient to have a way to compute the hydrogen production that varied with the load (as it will be seen in Section 7, this will have an impact in the system B with the amount of batteries selected by the OS), and so it was necessary to have an efficiency vs partial load curve. A general PEM electrolyzer curve was obtained by interpolating the curve used by Calado et al. [7], that they extrapolated from a load-efficiency curve displayed in the IRENA's report [24] for multiple existing electrolyzers. Current PEM efficiency ranges between 70% and 90%, while it is foreseen to reach 93% in 2030 [13], thus considering, the interpolated curve has been shifted up to reach 90% as peak efficiency for the 2030 efficiency scenario **[Fig.3.8]**. These values are only those of the maximum efficiency (while those at nominal load are lower) and are slightly lower than those given by Dinh et al. in [13], since it was chosen to follow a more precautionary approach, underestimating the hydrogen production, either for

the uncertainties that comes from this interpolation, and to counterbalance all the intrinsic simplifications of the models that do not take into account all the parameters that would be involved in a more realistic simulation.

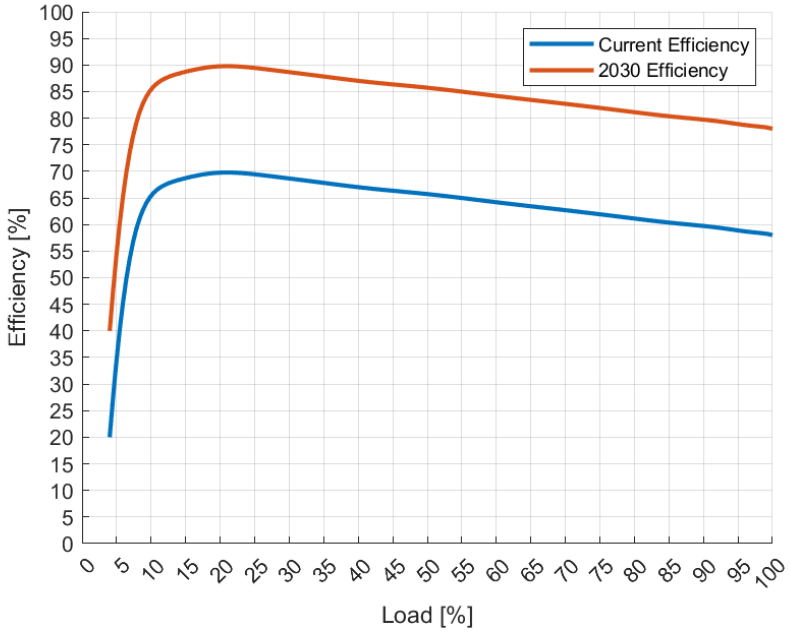

Figure 3.8: Electrolyzer's efficiency-load curve

Additionally, it is also considered the power consumption of the other elements that are part of the electrolyzer system, but that do not partake to the electrolysis process: the water desalinisation system, the cooling system, the external compression system and the dryer.
In order to properly function, the electrolyzers need water with a high degree of purity. However, being located in an offshore platform, the supply of fresh water is problematic, therefore it is required to use sea water. This has first to be desalinised by a reverse osmosis process by consuming electricity to strongly reduce the presence of chlorine ions in it (the production of chlorine gas would compete with the main reaction and lead to corrosion and safety issues). The extra power employed is much lower than that consumed for the electrolysis reaction, and it can be neglected [20] [19].
An higher operating temperature has a positive impact on the performances of the cell by improving the polarisation curve by increasing the exchange current density [14] and reducing the reversible cell voltage [33], but at the same time it affects the durability of the system by accelerating the corrosion processes, and

increasing the permeation rate of hydrogen through the polymeric membrane, accumulating on the oxygen gas, thus leading to concerning safety risks [33] [19]. Therefore it is necessary to control the temperature by intervening on the feed water temperature, or through an heat exchanger. The consumption of the cooling system has been estimated as $0.38\,kW/kg_{H_2}$ [19].
The hydrogen has be sent to the pipeline that will bring it from the offshore platforms to the mainland. It is possible to increase the operating pressure inside the electrolyzer, but this would then determine a decrease in the efficiency, related to the necessity of heaving a thicker membrane that would then compromise the gas permeation [19]. To avoid this problem it is then placed an external compressor unit, that rises the pressure from the outlet of the electrolyzer (30 bar), to the pipeline pressure of 60 bar [12]. The power consumption in that sense has been estimated as $0.88\,kW/kg_{H_2}$ [19].
Finally it is also considered the power consumption of the dryer, necessary to decrease the humidity content in the hydrogen outflow, as $0.5\,kW/kg_{H_2}$ [19].
The overall external power consumption is $p_{con} = 1.76\,kW/kg_{H_2}$, and in the model the additional power consumption is calculated as:

$$P_{con,ext} = H_2 \cdot p_{con} \tag{3.9}$$

3.3 Energy Storage System

The inclusion of an energy store system is fundamental for two reasons: first of all, being the hydrogen production system coupled with a fluctuating energy source, it provides it a way to better exploit the power produced, accumulating it during periods of abundance (when the production exceed the installed electrolyzers power), to feed them during scarcity times (allowing a reduction in the necessary H2S installed power), and secondly, in that way it is possible to keep the electrolyzers in operating conditions, limiting the ON/OFF cycles preserving their durability.
Three main technologies have been analysed, to choose the best one for the project. The first of them is the Lead-Acid battery, a mature and widespread technology with the main advantage of being available at the lowest cost of the three. However, it has been proven to not be particularly suitable in utility scale

power system, due to its inability to withstand either deep discharges or long periods without being charged [6]. Therefore the choice lies between Lithium-Ion and Redox Flow batteries. Papadopoulos et al. [30] have investigated the possibility of increasing the utilisation factor of a wind park in Belgium, by adding an hydrogen storage system coupled with an electrochemical storage. They compared the usage of redox flow battery with lithium NMC (Nichel Manganese Cobalt) and found out that redox batteries could endure more cycles with a negligible capacity fade. However, they preferred to them the Li-ion batteries, due to a lower cost and for their higher efficiency. Redox batteries can withstand prolonged charge/discharge periods with great DOD (Depth Of Discharge), without the risk of of deterioration, and also they rely at lesser extent in rare materials, nevertheless, for their higher cost, and for being still in their initial stage of commercialisation [6], Lithium-Ion was chosen for this project.
Lithium-Ion batteries present higher energy and power density, longer life and better efficiency than Lead-Acid batteries [4], making them more suitable for RES coupling. Currently NMC is the dominating technology, but in the following years Lithium Nickel Cobalt Aluminum (NCA) and Lithium Iron Phosphate (LFP) are expected to increase their market share [6].

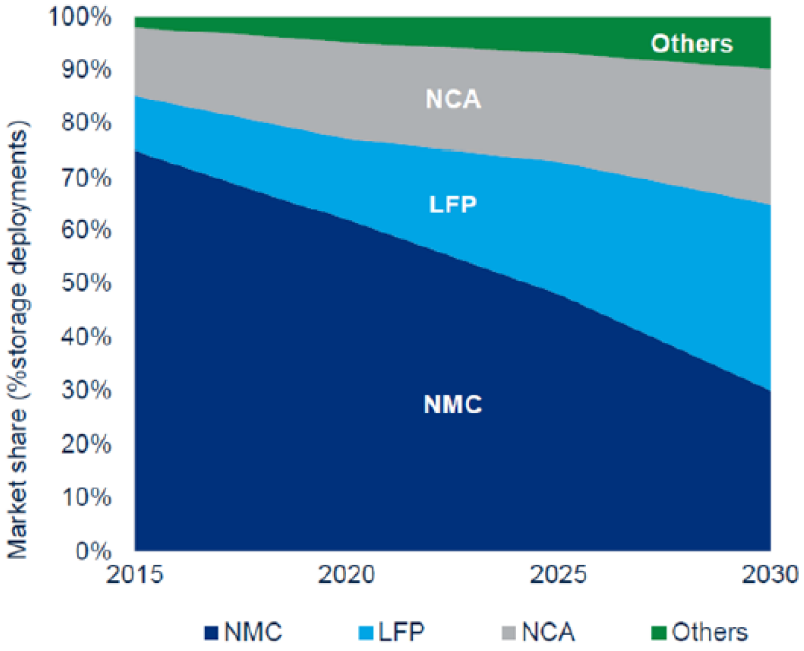

Figure 3.9: Lithium-ion battery chemistry market share forecast
From the USAID report [6]

Additionally, according to [39] LFP are about 10% less costly than NMC on a \$/kWh basis. Thus, given all the above statements, the technology chosen was Lithium Iron Phosphate batteries.

3.3.1 Modelling the ESS

For considerations similar to those in Section 3.2.1, it was opted for a simplified model, both because a detail dynamic model with a realistic battery control system would have been out of the scope of the project, and because it would have made the final simulations too heavy in terms of computative effort.
In a real case, the ESS would be composed of a multitude of battery banks connected in parallel and series, governed by control system able to optimise their functioning, and preserving their durability. But for the reasons above, it is instead modelled as a virtually big single battery unit, and its size S_{Bat} is defined as

$$S_{Bat_{kW}} = 500kW \cdot BSF \tag{3.10}$$

$$S_{Bat_{kWh}} = S_{Bat_{kW}} \cdot 2h \tag{3.11}$$

with $S_{Bat_{kW}}$ = the size of the battery in terms of power capacity, 500 kW is the minimum battery size allowed (and S_{Bat} is a multiple of it), BSF is the Battery Size Factor, a factor that determines the final capacity of the ESS and is the decision variable optimised inside the OS along with the number of electrolyzers. To get the capacity in terms of energy stored, $S_{Bat_{kW}}$ is multiplied by 2 hours which is the nominal discharging time (the time that takes to the battery to completely deliver all its energy while discharging itself at nominal power). Only the equation (3.10) is used inside the model, while the nominal discharging time is used to find the costs associated to it (see Chapter 5.2).
The DOD of the battery has to be limited to 80% [30], therefore the boundaries of the State of Charge (SOC) are set as SOC_{min} = 20% and SOC_{max} = 100%. The model can operate in three different conditions, Charging mode, Discharging mode and Idle mode (when no power is delivered, and just selfdischarge happens). It finds at the current time step the $SOC(t)$ by starting from the SOC of the previous step $SOC_0(t)$ [36]:

$$SOC(t) = \begin{cases} SOC_0 \cdot (1 - \delta_{Bat}) + \left(\eta_{Bat} \cdot \frac{P_{char}}{S_{Bat}}\right) & Charge\ Mode \\ SOC_0 \cdot (1 - \delta_{Bat}) + \left(\eta_{Bat} \cdot \frac{P_{disch}}{S_{Bat}}\right) & Discharge\ Mode \\ SOC_0 \cdot (1 - \delta_{Bat}) & Idle\ Mode \end{cases} \tag{3.12}$$

with P_{char} the power charged into the battery, P_{disch} the power discharged from the battery, δ_{Bat} the self discharging rate and η_{Bat} the charge/discharge efficiency. Then the energy that can be deployed by the battery $E_{Bat_{av}}(t)$ after that time step, is obtained as follows:

$$E_{Bat_{max}} = S_{Bat} \cdot BSF \cdot SOC_{max} \tag{3.13}$$

$$E_{Bat_{min}} = S_{Bat} \cdot BSF \cdot SOC_{min} \tag{3.14}$$

$$E_{Bat_{av}}(t) = \left(E_{Bat_{max}} \cdot SOC(t) - E_{Bat_{min}}\right) \cdot \eta_{conv,Bat} \tag{3.15}$$

with $E_{Bat_{max}}$ and $E_{Bat_{min}}$ the maximum and minimum energy that can be contained inside the battery, and $\eta_{conv,Bat}$ the efficiency of the AC/DC converter.

4 Control System

The components described and modelled in Section 3, are connected together and coordinated by a Control System (CS), that decides where to deploy the power fluxes based on certain set of rules. The work of Tebibel [36] and Atteme et al. [5], have been a starting point in the coding of the control system here proposed. The similarities with their works have been assimilated and then adapted to fit into this particular situation (especially for the presence of a pipeline instead of storage tanks, and for the logic used here to operate the electrolyzers). Two different control methodologies have been built in order to be later compared. The first one does not limit the ON/OFF cycles of the electrolyzers stacks, called **System A**, and the other obtained from the previous one, sets a constrain to the daily ON/OFF cycles of the electrolyzers, and divides them into two different categories, called **System B**.

4.1 System A

In this control strategy, the ON/OFF cycles of the stacks are not constrained, and, based on the power available, they are fed in succession, by trying to keep them working at nominal load, with just one at partial load, while the remaining are turned OFF.
To the control system are sent two types of input that it utilises to perform its calculations: fixed inputs, that are those related to the characteristics of the electrolyzer and the ESS, the number of electrolyzers n_s and the size of the ESS (the BSF), that make up the system configuration that is currently being

evaluated **[Tab.4.1]**, and a variable input, which is the hourly power provided by the wind farm $P_{WF}(t)$.

Electrolyzer	
Number of electrolyzers	
Minimum power input	100 kW
Nominal load	2 MW
Efficiency at nominal load	58% (current efficiency) 78% (2030 efficiency)
DC converter efficiency	93% [13]

ESS	
ESS size	
Self discharge rate	$83,33 \cdot 10^{-4}$ % [36]
Charge/Discharge efficiency	96% [40]
Converter efficiency	95% [36]
Minimum power input	3 kW
Nominal power	500 kW
Minimum SOC	20%
Maximum SOC	100%

Table 4.1: Input information in the control system

The minimum and maximum power that can be sent to the H2S, during each time step are defined as:

$$IN_{el_{min}} = \frac{P_{el,min} \cdot n_s/2}{\eta_{DC_{el}}} \tag{4.1}$$

$$IN_{el_{max}} = \frac{P_{el,nom} \cdot n_s}{\eta_{DC_{el}}} \tag{4.2}$$

The CS evaluates the wind power available, and then it chooses how to use it by following one of three possible scenarios by comparing it with $IN_{el_{min}}$ and $IN_{el_{max}}$, and checking at each time step the state of charge of the ESS. The flow chart of the control logic adopted inside System A is shown in **[Fig.4.2]**.

1. **LOW POWER SCENARIO** $P_{WF}(t) < IN_{el_{min}}$

The wind power is not able to provide the stacks with enough power just

by itself and it needs the support of the ESS. Thus, the CS evaluates the Power available $P_{av}(t)$ as the sum of the power from the wind farm and the one that can be deployed by the ESS, defined as:

$$P_{Bat_{av}}(t) = (P_{Bat}(t) - E_{Bat_{min}} \cdot t) \cdot \eta_{conv,Bat} \tag{4.3}$$

In relation to $P_{av}(t)$ there are two available paths:

(a) ESS IN DISCHARGE MODE $P_{av}(t) \geq IN_{el_{min}}$

The ESS is discharged and delivers $P_{Bat_{av}}(t)$ to the stacks, which are put into operation at nominal load when possible, otherwise at partial load, or they are just turned OFF.

(b) ALL ELECTROLYZERS OFF $P_{av}(t) < IN_{el_{min}}$

i. ESS IN CHARGE MODE $SOC_{Bat} < SOC_{max}$

The extra power is used to fill the storage system, that will use it during the **LOW POWER SCENARIO** or the **PARTIAL LOAD SCENARIO**.

ii. DUMP LOAD $SOC_{Bat} \geq SOC_{max}$

The ESS has already been filled and there is nothing that can exploit the power that is insufficient for the H2S. This has then to be sent to a dump load and that power is lost.

2. **HIGH POWER SCENARIO** $P_{WF}(t) > IN_{el_{max}}$

$P_{WF}(t)$ in this case feeds all the stacks at nominal power. Concerning the remaining extra power, similarly to what happens in the **LOW POWER SCENARIO**:

(a) ESS IN CHARGE MODE $SOC_{Bat} < SOC_{max}$

(b) DUMP LOAD $SOC_{Bat} \geq SOC_{max}$

3. **PARTIAL LOAD SCENARIO** $IN_{el_{min}} \leq P_{WF}(t) \leq IN_{el_{max}}$

This an intermediate situation, where the power of the wind is not enough to cover alone the power demand of the total electrolyzer installed power, but is also higher than the minimum power input. The CS evaluates the amount of power available from the WF, and that deployable by the assisting ESS, then:

(a) Nominal Load $P_{av}(t) \geq IN_{el_{max}}$

All the electrolyzers can be fed at nominal load, and the ESS is discharged to provide the residual quantity of power unmet by the WF.

(b) Partial Load $P_{av}(t) \geq IN_{el_{max}}$

The ESS is discharged, but only few electrolyzers can be fed. The CS powers them in cascade, by feeding to each of them, one by one, the rated power until there is no power left. Therefore a certain amount of electrolyzers will be working at nominal power, one of them at partial load, and the remaining will be turned OFF. The control scheme for the electrolyzers is shown in detail in **[Fig.4.1]**.

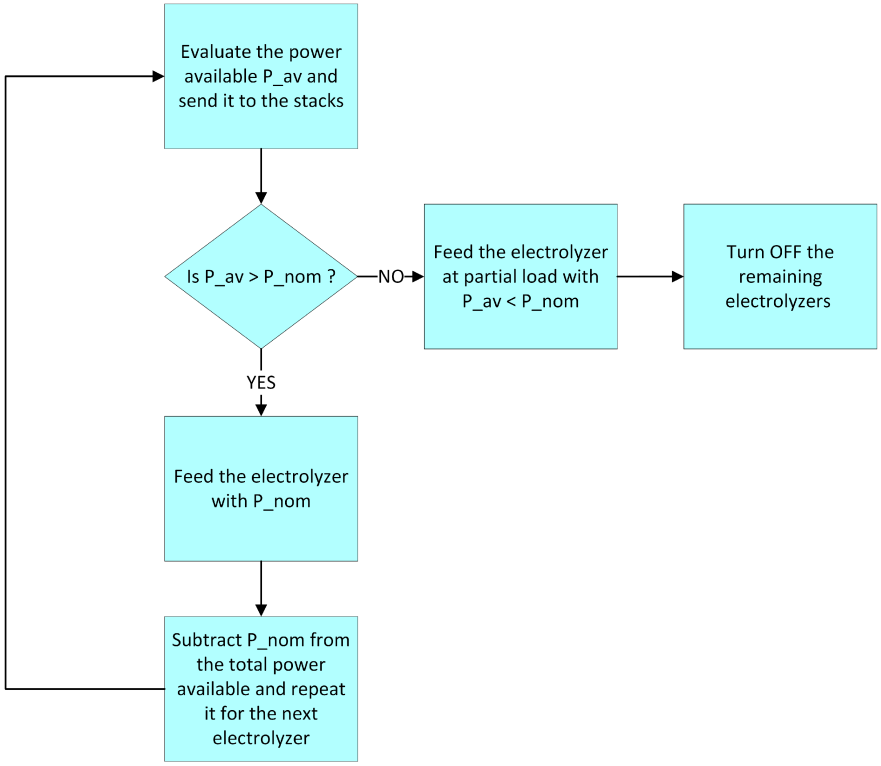

Figure 4.1: Stacks control flow chart in System A

The control scheme simulates a real physical situation that involves the exchange of power between the wind farm, the electrolysers, the ESS and the dump load. However, the implementation in the software does not match it exactly, and creates a virtual exchange of power fluxes (the information fluxes) that do not actually happen in reality. For instance, after all the power available from the WF and the ESS has been calculated, the software sends all of it to the electrolyzers, which then give back the amount they did not consume to the

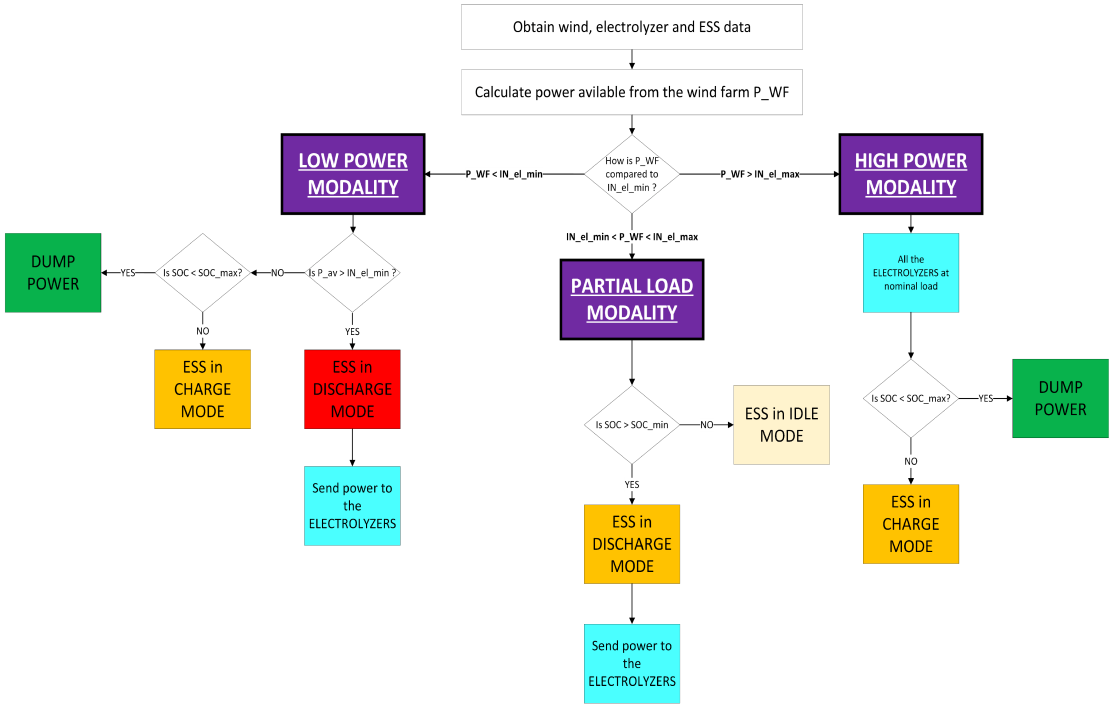

Figure 4.2: Flow chart of the control scheme of System A

In the chart the colours refers to: purple for the power scenarios, cyan for the electrolyzer component, red/yellow for ESS component in different modalities and green for the dump load.

battery, which only after that is discharged. The sequence inside the script is WF-Electrolyzers-ESS-Dump **[Fig.4.3]**.

This control scheme does not limit the daily ON/OFF cycles of the electrolyzers, and they are continuously turned on as long there is enough power. This has two consequences, the usage of batteries becomes less necessary to the system and also it might compromise the durability of the electrolyzer. The number of ON/OFF cycles that are allowed should be limited [38], so a variable has been introduced that evaluates for each stack the number of ON/OFF cycles per day exceeded, in respect to a threshold number (here the value of 5 has been chosen). This variable will be then used inside the LCOH calculation (see Chapter 5.2).

4.2 System B

As will be discussed in Chapter 7, the main problem of System A is that its lack of limitation on the allowed ON/OFF cycles, leads the OS to prioritise the increase of the electrolyzers capacity, almost avoiding completely the usage of a storage system. Therefore, after several simulations with System A, a second

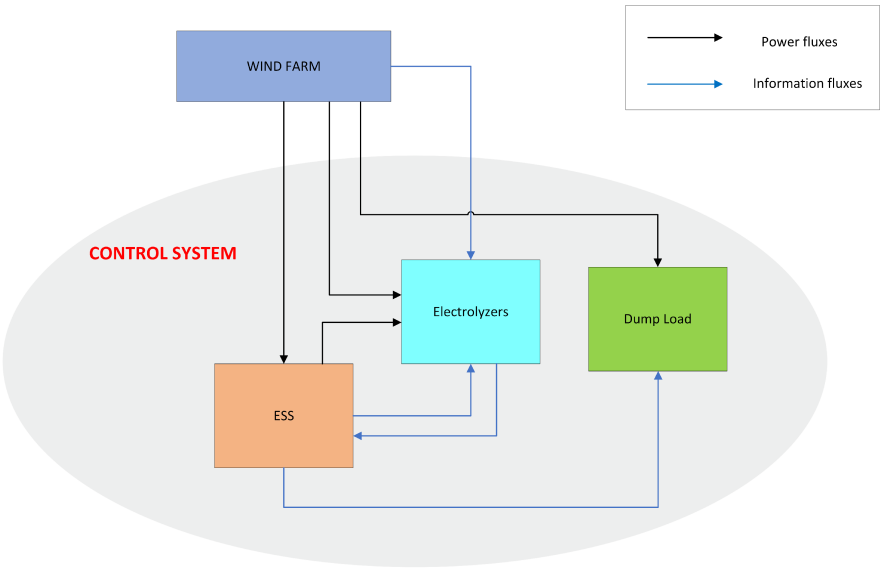

Figure 4.3: Control scheme layout

CS with a different control logic for the electrolyzers has been coded.
First of all, System B introduces the *Baseload Electrolyzers*, which is the maximum number of electrolyzers able to work at nominal load for at least the 80% of the time. For the chosen location, the wind and the WF characteristics shown in Chapter 3.1, the baseload electrolyzers n_{base} are 47, for a total capacity of 94 MW, from now on indicated as BL. They are prioritised by the control system that maintains them always ON when possible, and they are not subject to any constraints on their daily ON/OFF cycles. The same does not apply to the remaining electrolyzers, that cannot be turned ON and OFF for more that 5 times per day. It is given to them a constraint that allows them to function only either if they were ON in the previous time step, or if they have been OFF for the previous 5 hours, otherwise they must remain OFF. This is done for each time step, and the total number of electrolyzers that can work (n_{base} included) are called $n_{allowed}$.
At the beginning, it calculates $n_{allowed}$ and it finds the maximum and minimum power that can be sent to the H2S, defined as:

$$IN_{el_{min}} = \frac{P_{el,min}}{\eta_{DC_{el}}} \tag{4.4}$$

$$IN_{el_{max}} = \frac{P_{el,nom} \cdot n_{allowed}}{\eta_{DC_{el}}} \tag{4.5}$$

then, it evaluates $P_{Bat_{av}}$ as in Equation (4.3). With all these information, it proceeds following two possible strategies, the **LOW POWER SCENARIO** or the **HIGH POWER SCENARIO** [Fig.4.4]:

1. **HIGH POWER SCENARIO** $P_{WF}(t) \geq IN_{el_{max}}$

   $P_{WF}(t)$ in this case feeds all the $n_{allowed}$ stacks at nominal power, while the other $n_s - n_{allowed}$ remain OFF. According to the SOC of the ESS, the CS has two alternatives:

   (a) ESS IN CHARGE MODE $SOC_{Bat} < SOC_{max}$

   The extra power is used to fill the storage system, that will then use it during the **LOW POWER SCENARIO**.

   (b) DUMP LOAD $SOC_{Bat} \geq SOC_{max}$

   The ESS is already filled and there is nothing that can use the exceeding power. This has then to be sent to a dump load and that power can be considered wasted.

2. **LOW POWER SCENARIO** $P_{WF}(t) < IN_{el_{max}}$

   The wind power is not able to provide all the stacks with enough power just by itself, and the ESS has to be discharged (if $SOC_{Bat} > SOC_{min}$). Based on the available power, it chooses between two alternatives:

   (a) BASELOAD CASE $P_{av}(t) \geq BL$

   The n_{base} electrolyzer can be all kept ON working at maximum load, while for the remaining electrolyzers $n_{rem} = n_{allowed} - n_{base}$:

   i. Nominal Load $P_{av}(t) \geq P_{el,nom} \cdot n_{rem}$

   All the n_{rem} electrolyzers are fed at nominal power.

   ii. Partial Load $P_{el,min} \cdot n_{rem} < P_{av}(t) \leq P_{el,nom} \cdot n_{rem}$

   All the n_{rem} electrolyzers remain turned ON, but the power is split between them and they work at partial load.

   iii. Minimum Load $P_{el,min} \geq P_{av}(t) \geq P_{el,min} \cdot n_{rem}$

   There is not enough power both from the WF and the ESS to maintain every n_{rem} electrolyzer ON, so the CS finds the maximum number of those that can work at minimum load and turns OFF the others

   (b) **BELOW BASELOAD CASE** $P_{av}(t) < BL$

   This is the low power scenario when the power produced by the WF,

combined by the ESS is not able to sustain the operation at nominal load of the n_{base} stacks that make up the BL. Therefore, there are two possibilities, that are analogue to what is described in the previous case. All the n_{rem} remain OFF.

i. Partial Load $\quad P_{el,min} \cdot n_{base} < P_{av}(t) \leq P_{el,nom} \cdot n_{base}$

All the n_{base} electrolyzers remain turned ON, but the power is split between them and they work at partial load.

ii. Minimum Load $\quad P_{el,min} \geq P_{av}(t) \geq P_{el,min} \cdot n_{base}$

There is not enough power to maintain all the n_{base} electrolyzers ON, so the CS finds the maximum number of those that can work at minimum load and turns OFF the others. Differently from the non-baseload-stacks, the n_{base} that are turned OFF during that time step, are allowed to be turned OFF in the following time step if the power is enough, ignoring the ON/OFF cycle constraint.

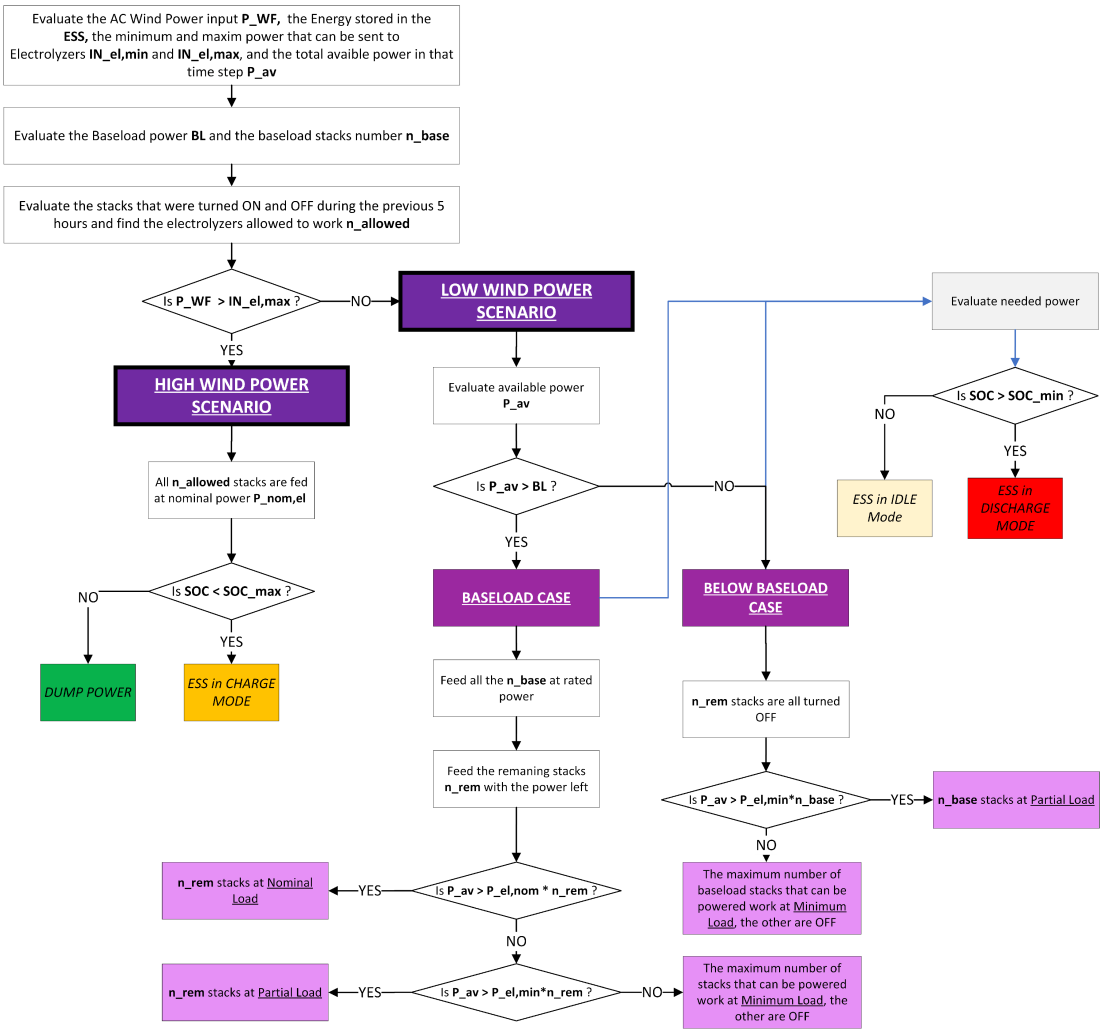

Figure 4.4: Flow chart of the control scheme of System B

5 Multiobjective Functions

The system's components, and their ruling control system, make up the Physical Component of the Optimisation System. The other element of the OS is the Decision Component, that by using a set of algorithms balances the decision variables to optimise two, or more, contrasting Objective Functions (OF).
The choice of which objective function to use is fundamental, since it is the only way to properly size the WtHS. However, it was not yet clear in the earliest stages of project which OFs would have been the most suitable to use in that case. Similar cases have already been discussed in the literature, nevertheless, they differ in a way that it becomes impossible to follow the same exact approach. Thus, several suggestions for the OFs have been taken from the literature to be combined together and to find the optimisation strategy that gives the most effective results. Here they are all presented and explained.

5.1 Capital Expenditure

The Capital Expenditure (CAPEX) is the funds that are necessary to acquire to build all the elements that are part of the Wind-to-Hydrogen system. It is a fixed cost which is incurred at the very beginning, from the earliest stage of the project. Its minimisation inside the OS leads to obtaining a sizing combination that reduces the costs as much as possible. Here, the cost sources are four: the wind farm, the hydrogen system, the energy storage system and finally, the pipeline. Therefore the CAPEX of the project is defined as:

$$CAPEX = CAPEX_{WF} + CAPEX_{H2S} + CAPEX_{ESS} + CAPEX_{pipeline} \quad (5.1)$$

As it was stated in the hypothesis, all the costs are referred to 2030, and they are expected to decrease in relation to the increase in the total installed capacity and to the research and development efforts.

5.1.1 CAPEX of the Wind Farm

The future costs $COST_f$ have been estimated by Dinh et al. [12] starting from the present costs $COST_p$ through the experience curve theory as:

$$COST_f = COST_P \cdot \left(\frac{CCf}{CCp}\right)^{\frac{log(1-LR)}{log(2)}} \quad (5.2)$$

with LR the learning rate **[Tab.5.1]** and CC the future and present cumulative capacities [25] [22] **[Tab.5.2]**.

Offshore wind turbine	0,07
Foundation	0,025
Grid connection	0,14
Other components	0,13

Table 5.1: Learning rates

Year	Capacity [GW]
2020	34,4
2021	54,3
2030	228

Table 5.2: Cumulative capacities

A detailed way of estimate the $CAPEX_{WF}$ have been described by [12], and it is composed of six parts, the costs related to development and consent phase, to the substation and the array cable, and those connected to the construction of the offshore wind farm (the cost of the turbines, for the foundations and installation):

$$CAPEX_{WF} = COST_{D\&C} + COST_{Turbines} + COST_{Foundation} + \\ + COST_{Installation} + COST_{Substation} + COST_{Arraycable} \tag{5.3}$$

$$COST_{D\&C} = Price_{D\&C} \cdot C_{WF} \tag{5.4}$$

$$COST_{Substation} = Price_{Substation} \cdot C_{WF} \tag{5.5}$$

$$COST_{Arraycable} = Price_{Arraycable} \cdot C_{WF} \tag{5.6}$$

To estimate the cost of the turbine, a linear regression function has been used [12] that takes into consideration the cost reduction in economies of scale. Equation (5.7) is a function of the size of the turbines in the wind farm S_T, and its overall capacity C_{WF}. The other cost components accounts for the actual construction of the WF in that specific site. Equation (5.8) estimates the cost of building the foundations for the offshore turbines. Jacket foundations are used when the water depth is between 30 and 60 meters [12] (the average water depth in Kilmichael Point is 39m). Inside it, also the cost of the vessel carrying the foundations is evaluated, considering its speed, the distance from the port, the length of the round trip, the installation time and the foundations carried per trip. Finally, equation (5.10) accounts for the installation costs of the turbines, and it is calculated similarly to how it was done for the foundation costs. In **[Tab.5.3]** are shown the values of the parameter used in the equations taken from [12].

$$COST_{Turbines} = \left(1.6 - \frac{1.9}{S_T}\right) \cdot (C_{WF})^{0.9984} \tag{5.7}$$

$$COST_{Foundation} = COST_{mf} + COST_{f_{Transport}} + COST_{f_{Install}} = \\ = Price_{mf} \cdot C_{WF} + \left(n_T \cdot T_{f_{install}} + \frac{n_T}{n_{f_{trip}}} \cdot T_{to\,site}\right) \cdot Price_{f_{Vessel}} \tag{5.8}$$

$$T_{to\,site} = \frac{2 \cdot D_{Port}}{V_{Vessel} \cdot h_{work}} \tag{5.9}$$

$$COST_{Installation} = \left[n_T \cdot T_{t_{install}} + \frac{n_T}{n_{tur_{trip}}} \cdot T_{to\,site} \right] \cdot Price_{f_{Vessel}} \tag{5.10}$$

	Present Value	Value 2030	Unit
Price Developing and Consenting phase $Price_{D\&C}$	0,188	0,128	M€/MW
$Price_{Substation}$	0,14	0,092	M€/MW
$Price_{Arraycable}$	0,041	0,026	M€/MW
Manufacturing cost Jacket $Price_{mf}$	0,442	0,409	M€/MW
Daily price of the vessel $Price_{Vessel}$	0,15	0,102	M€/day

	Value	Unit
Speed of the installation vessel V_{Vessel}	20	km/h
Distance from the port D_{Port}	18,6	km
Installation time Jacket $T_{f_{Install}}$	3	days
Installation time $T_{t_{Install}}$	2	days
Working hours h_{work}	24	hours
Number of foundations that can be carried $n_{f_{Trip}}$	5	
Number of trips of the vessel for each turbine $n_{tur_{Trip}}$	5	

Table 5.3: Parameters used in the calculation of $CAPEX_{WF}$

As the characteristics of the WF are the same for both the control systems and in each scenario, $CAPEX_{WF}$ is the only term of the final CAPEX that remains constant for each ESS and H2S configuration, and it is $\sim 964M€$. The impact of each component of $CAPEX_{WF}$ in the final value is shown in **[Fig.5.1]** and **[Tab.5.4]**. The cost for the turbines and for the foundations are the predominant ones, making up more that the 3/4 of the final CAPEX of the WF.

5.1.2 CAPEX of the Energy Storage System

The CAPEX of the battery system is evaluated as [43] [39]:

$$CAPEX_{ESS} = C_{PCS} + C_{BOP} + C_{Stor} \tag{5.11}$$

where C_{PCS} is the Power Conversion System (PCS) cost, C_{BOP} the Balance of

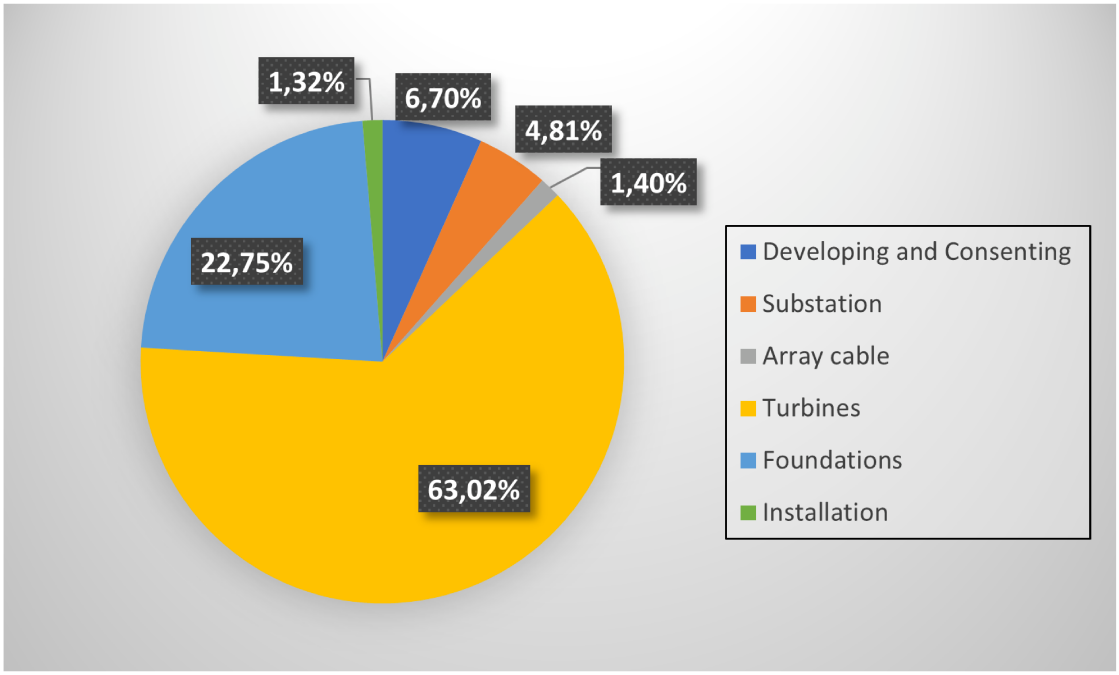

Figure 5.1: Pie chart of the CAPEX of the Wind Farm

TOTAL	$964,46M€$	
Turbines	$607,82M€$	$63,02\%$
Foundations	$219,41M€$	$22,75\%$
Developing and Consenting	$64,61M€$	$6,70\%$
Substation	$46,39M€$	$4,81\%$
Array cable	$13,52M€$	$1,40\%$
Installation	$12,69M€$	$1,32\%$

Table 5.4: Contributions to the $CAPEX_{WF}$ in absolute and percent terms.

Plant cost, and C_{Stor} the cost of the energy storage system.
C_{Stor} is the cost related to the component of the BESS that stores the energy, and includes battery module (with the costs of electrodes, electrolytes and separators), rack, and battery management system (BMS) [39]. Since the AC power coming from the wind farm needs to be converted into DC power to charge the battery (and the contrary when the battery is discharged), the cost component C_{PCS} involves the cost of the inverter, the packaging, and the inverter controls. The values used to calculate the CAPEX are shown in **[Tab.5.5]** and are taken from [39] for the costs at 2030 scenario for a lithium-ion LFP ESS 10 MW system. The CAPEX is $559,03\,\$/kWh$ and it has been converted from USD to EURO by multiplying it by a $0,91$ exchange rate.

DC Storage Block	115,31	$/kWh
DC Storage BOS	32,41	$/kWh
Power Equipment	64,62	$/kW
C&C	5,78	$/kW
System Integration	43,8	$/kWh
EPC	52,88	$/kWh
Total Installed Cost	559,03	$/kWh

Table 5.5: Cost components of the $CAPEX_{ESS}$

5.1.3 CAPEX of the Hydrogen System

The CAPEX of the hydrogen system accounts only for the cost of the stacks and of the compressors needed to achieve the suitable pressure to send the hydrogen to the pipeline. The cost of the compressor is related to its power $P_{Compressor}$, which is a function of the flow rate of hydrogen Q [12]. As Q, it has been taken the output flow rate at nominal load. The parameters used in the calculations are shown in **[Fig.5.6]** (except from Q, they come from [12]).

$$CAPEX_{H2S} = CAPEX_{Electrolyzers} + CAPEX_{Compressors} \tag{5.12}$$

$$CAPEX_{Electrolyzers} = CAPEX_{El/MW} \cdot n_s \cdot P_{El,nom} \tag{5.13}$$

$$P_{Compressor} = Q \cdot \frac{R \cdot T \cdot Z}{\eta_{com} \cdot M_H} \cdot \frac{N \cdot \gamma}{\gamma - 1} \left[\left(\frac{p_o}{p_i} \right)^{\frac{\gamma-1}{N \cdot \gamma}} - 1 \right] \tag{5.14}$$

$$CAPEX_{Compressors} = n_s \cdot 12600 \cdot \left(\frac{P_{Compressor}}{10}^{0.9} \right) \tag{5.15}$$

5.1.4 CAPEX of the Pipeline

The hydrogen is sent from the offshore platforms to the mainland through subsea pipelines. The CAPEX of the pipelines is a function of the maximum hydrogen production rate $Q_{tot} = Q \cdot n_s$, and of the distance from the injection point D_{inject} (which is 46,5 km for Kilmichael Point) [12].

$CAPEX_{El/MW}$	0,6 M€/MW
Hydrogen flow rate Q	0,0078 kg/s
Isentropic efficiency γ	1,4
Compressor efficiency η_{com}	75%
Hydrogen molecular mass M_H	2,016 g/mol
Ideal gas constant R	8,314 J/mol K
Temperature at inlet T	310 K
Compressibility factor Z	1,03
Outlet electrolyzer pressure p_i	30 bar
Pipeline operating pressure p_o	60 bar

Table 5.6: Parameters used in the calculation of $CAPEX_{H2S}$

$$CAPEX_{pipeline} = \left(16000 \cdot \frac{Q_{tot}}{\rho \cdot v \cdot \pi} + 1197.2\sqrt{\frac{Q_{tot}}{\rho \cdot v \cdot \pi}} + 329\right) \cdot D_{inject} \tag{5.16}$$

with $v = 15\,m/s$ the average fluid velocity and $\rho = 8\,kg/m^3$ the mass density.

5.2 Levelized Cost Of Hydrogen

The Levelized Cost of Hydrogen(LCOH) is a very efficient way to estimate the costs in relation to the final product, the hydrogen, that is the main purpose of the system. The costs can be classified into three categories, the CAPEX, the OPEX (OPErational EXpenditure, the costs related to the maintenance of the system) and the DECEX (DECommissioning EXpenditure, the cost related to the decommissioning of the systems at the end of their life cycle). These are then equally subdivided to each kilogram of hydrogen produced during the all expected operating period of the WtHS. Being $life = 25\,years$ the project's lifetime and $r = 5\%$ the interest rate, the LCOH is defined as:

$$LCOH = \frac{CAPEX + \sum_{n=1}^{life} \frac{OPEX_i}{(1+r)^i} + DECEX}{\sum_{n=1}^{life} H_{2i}} \tag{5.17}$$

5.2.1 Operational Expenditure

The OPEX for the WF, the pipeline and the H2S, is expressed as a function of the corresponding CAPEX (for the last one there is also a Replacement cost term) [12], while the OPEX of the ESS is function of the installed capacity [39]. The values used have been included in **[Fig.5.7]**.

$$OPEX_{H2S} = OPEX_{Electrolyzer} + OPEX_{Compressor} + COST_{El,Replace} \quad (5.18)$$

$$OPEX_{Electrolyzer} = OPEX_{Electrolyzer_{\%}} \cdot CAPEX_{Electrolyzer} + COST_{Replace,El} \quad (5.19)$$

$$OPEX_{ESS} = (OPEX_{ESS_{kW}} \cdot BSF \cdot S_{Bat}) + (Cost_{Replace,ESS} \cdot \frac{life}{rep_{year}}) \quad (5.20)$$

where rep_{year} are the years after which the batteries have to be replaced.

$OPEX_{WF_{\%}}$	3	$\%CAPEX_{WF}$
$OPEX_{Electrolyzer_{\%}}$	2	$\%CAPEX_{Electrolyzer}$
$OPEX_{Compressor_{\%}}$	3	$\%CAPEX_{Compressor}$
$OPEX_{Pipeline_{\%}}$	2	$\%CAPEX_{Pipeline}$
$OPEX_{ESS_{kW}}$	2,37	\$/kW
$Cost_{Replace,ESS}$	295,44	\$/kW
$COST_{Replace,stack}$	0.15	M€/MW
rep_{year}	10	years

Table 5.7: OPEX calculation values

Excess Penalty

Inside the OPEX of the Electrolyzers an other parameter has been added to the replacement cost of the electrolyzer, the $COST_{Excess}$, a penalty cost factor related to the excessive daily ON/OFF cycles, both to account for the degradation of the machine, but also to see if the Optimisation System in its presence would

try to increase the capacity of the ESS to tackle this extra cost. The total number of time in which the constraint is exceeded is indicated by the term n_{Excess}, which is divided by the number of days in a year and multiplied by the replacement cost of a single stack to make the $COST_{Excess}$.

$$COST_{Replace,El} = (COST_{Replace,stack} + COST_{Excess}) \cdot n_s \cdot P_{El,nom} \tag{5.21}$$

$$COST_{Excess} = \frac{n_{Excess}}{365} \cdot COST_{Replace,stack} \tag{5.22}$$

5.2.2 Decomissioning Expenditure

Analogously, the DECEX is calculated as a percentage of the CAPEX [12]. On the other hand, for the batteries it was estimated that in 2030 the revenues from recycling, combined with the costs of disposal, will make the DECEX of the batteries drop to 0 [39].

$DECEX_{WF_{\%}}$	5	$\%CAPEX_{WF}$
$OPEX_{H2S_{\%}}$	2	$\%CAPEX_{H2S}$

Table 5.8: DECEX calculation values

5.3 Energy Dump Possibility

Proposed by [36], the Energy Dump Possibility (EDP) is defined as

$$EDP = \frac{E_{Dump}}{E_{WF}} \tag{5.23}$$

where E_{Dump} is the amount of energy that has been sent to the dump load instead to the stacks or to the ESS during each time step. It measures the efficiency of the system in terms of exploiting the energy from the wind resource. By optimising it, the system will try to improve the size of the WtHS and of the ESS, to reduce the amount of time when the E_{WF} cannot be fully utilised.

5.4 Benefit Cost Ratio

The Benefit Cost Ratio BCR has been used by Kelly et al. [27] to size the a battery ESS in a microgrid. It is an economical indicator that compares the relative benefits with the relative costs of a project and it allows to give an overall idea if it can be profitable (if $BCRC > 1$) or not (if $BCRC < 1$) [2]. The following equations define the yearly and discounted benefits obtained by selling the hydrogen:

$$B_y = H2_{year} \cdot p_{H_2} \tag{5.24}$$

$$B_{disc} = \sum_{n=1}^{life} \frac{B_{yi}}{(1+r)^i} \tag{5.25}$$

the Benefit Cost Ratio is defined as:

$$BCR = \frac{B_{disc}}{C_{disc}} \tag{5.26}$$

p_{H_2} is the price at which the hydrogen is sold, at it is supposed it to be 7€ throughout all the project life, and C_{disc} are the discounted costs (the sum of CAPEX, OPEX and DECEX). By maximising it, the OS tries to find a combination of the BSF and the n_s that increases the profitability of the project. The algorithms described in Chapter 6 optimise the objective functions by minimising them, and since the BCR has to be maximised instead of being minimised, the actual function that is used in the OS is $1 - BCR$.

5.5 Conversion LCOH

Being the $CAPEX_{WF}$ the predominant part of the final value of the LCOH, but also a fixed cost independent on the actual size of the H2S and ESS, an other parameter has been introduced, called the Conversion LCOH, that is defined exactly as the LCOH, but that accounts only for the costs related to the conversion and hydrogen transportation apparatus, excluding the CAPEX of the wind farm from the calculation. It is used to minimise the contribution to the LCOH given

just by the H2S and the ESS. The CAPEX that is calculated to determine the CLOCH is called CCAPEX (Conversion CAPEX), and it refers to the Hydrogen System, the ESS and the pipeline.

6 Algorithms

After the coding of the Control System, that makes up the Physical Component of the Optimisation System, it was built the Decision System inside the OS, able to use the aforementioned to find the best configuration for the set of objective functions selected.
The Decision System is made up of three algorithms, NSGA-II, CRITIC and TOPSIS [41], that find the best possible configurations (the combinations of the sizing variables, here the number of the electrolyzers and the BSF) and then ranks them from the best to the worst.

6.1 Selection Algorithm: NSGA-II

The use of Non Sorted Genetic Algorithms (NSGA), has been widely explored and recommended in the literature for similar size optimisation problems [41] [5]. Given two or more parameters to size, and two or more objective functions to minimise, the NSGA through multiple iterations evaluates them, until it finds the Pareto front, the set of solutions for which it is impossible to improve an objective function without worsening the other. These solutions that have been found cannot be further improved, but the algorithm is not able to determine which one is better than the other. The algorithm used here is the NSGA-II, an improved version of the NSGA proposed by [8]. The code has been downloaded from https://it.mathworks.com/matlabcentral/fileexchange/65494-non-sorting-genetic-algorithm-ii-nsga-ii?s$_tid = FX_rc1_behav$, and it has been modified to be com-

patible with the other Matlab functions and scripts personally made.
The algorithm performs a selection based on an analogy to the evolutionary theory to find the best *individual* (the configuration), that has the best *genes* (the sizing variables). At the beginning a random *population* (a group of configurations) of size P_t is created. Then it is obtained Q_t from P_t by mixing and mutating the genes, and the overall population is R_t with double the size of P_t. At the end of the iteration only a population of the size of P_t, with the best genes will make it to the following *generation*. The value that have been used are 200 for the size of the population, 5% for the probability of mutation, and the number of generations (which is the number of total iterations) is 35.
In relation to the computational effort, the OS calculates 35 iterations, during which executes for each of the 200+200 individuals, the control system for 8760 times, corresponding to the number of hours in a year. Therefore, the total number of times the CS is put into operation for a single simulation is 122640000, and they take usually from 20 to 50 minutes to be completed. This validates the choice of coding a simplified system instead of a complex and detailed one, stated in Chapter 3.
The multiple phases occurring in the NSGA-II algorithm are schematised in **[Fig.6.1]**.

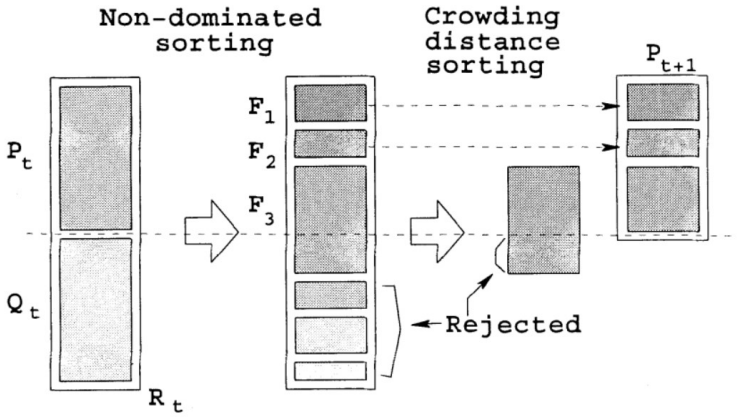

Figure 6.1: NSGA-II procedure
Courtesy from [8].

6.1.1 Non Dominated Sorting

In this first phase, all the individuals are subdivided into fronts. For each of them it is counted the number of times when it is *dominated* by an other individual. Being f1 and f2 the two target functions, and $A(x1, y1)$ and $B(x2, y2)$ the two individuals , B is dominated by A when ($x1 \leq x2$ and $y1 \leq y2$) and ($x1 < x2$ or $y1 < y2$). The individuals dominated by the same number of individuals are put together in a front and the fronts are ranked starting from the least to the most dominated. At every following generation, the population converges towards the Pareto front **[Fig.6.2]**

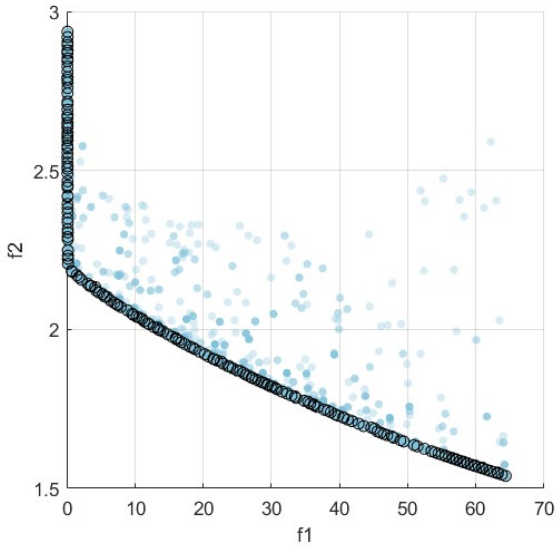

Figure 6.2: Evolving Pareto front

The points in light blue are the individuals that are dominated by other, while those circled in black are the non dominated ones that build up the Pareto front, for which is impossible to further reduce f1 without increasing f2, and vice-versa.

6.1.2 Crowding Distance Sorting Sorting

Only the first ranking fronts are passing to the next population, but there might be a front which would not be able to pass in its entirety (as it can be seen in **[Fig.6.1]**). Therefore it is used an other indicator, the crowding distance, to sort out the individuals in the front. It is calculated the distance for each individual for both the targets (the objective functions to minimise). The distance of a single individual is the sum of the distances referred to each

target, which are the ratio of the difference between the distance to the two neighbouring individuals, divided by the difference between the individuals with the maximum and minimum value of the target. The individuals are so ranked based on the highest distance values **[Fig.6.3]**.

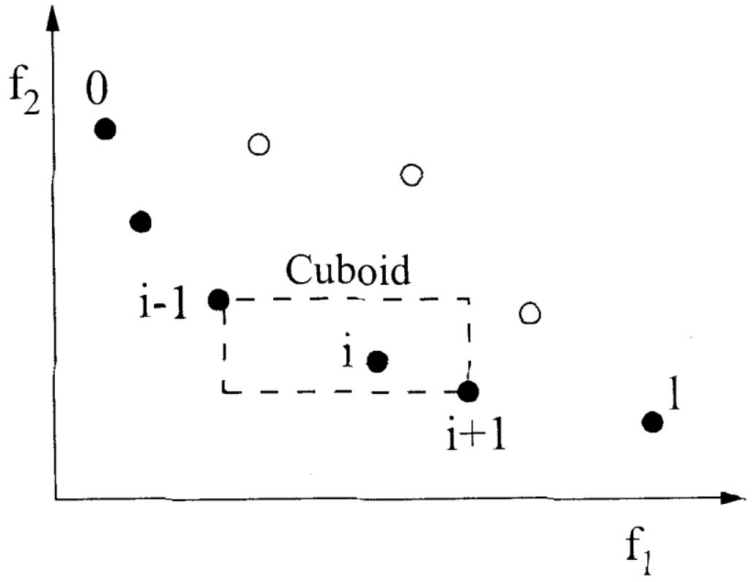

Figure 6.3: Crowding-distance calculation

Courtesy from [8].

6.1.3 Produce Offspring

After the population is selected, during the following iteration, the chosen population P_t is used to generate its offspring in the population Q_t. To create Q_t an other series of processes happens:

- **Tournament Selection**: the new *offspring* is generated by those that are considered the best *parents*. To find the two parents, the individuals are compared two by two. The one with highest ranking front (and highest crowding distance, if they both belong to the same front) is able to reproduce and generate an offspring.
- **Crossover**: the genes of the *child* are taken half from one parent, and half from the other.
- **Mutation**: with a certain selected probability mutation can happen. When it occurs, a random gene of the child is modified with a new random value.

Two types of Pareto front that have been found with this method are shown in **[Fig.6.4]**

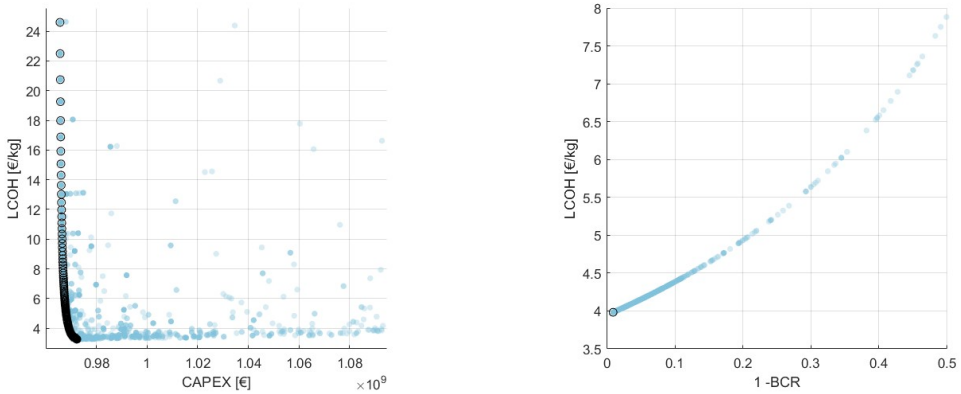

(a) CAPEX vs LCOH Pareto Front (b) BCR vs LCOH Pareto Front

Figure 6.4: Simulations comparison

Usually, the optimisation of a target function compromise the other (increasing the size of the electrolyzer up to a certain point reduces the LCOH, but increases the CAPEX) and therefore a Pareto front can be found. Sometimes the two targets can be optimised together and an improvement in one, improves also the other (minimising the LCOH maximises at the same time the BCR) and so, there is just one unique solution.

6.2 Weighting Algorithm: CRITIC

The NSGA produces only the solutions belonging to the Pareto front, but it does not give any clue about which solutions should be regarded as optimal in relation to the objective functions that have been minimised alongside. Thus, in the second part of the Decision Component of the OS, the algorithm have to weight (CRITIC) and rank (TOPSIS) these points.
The Criteria Importance though Intercrieria Correlation (CRITIC) has been first proposed by [11] and it was chosen by [41] among other weighting algorithms. It uses the standard deviation to measure the discreteness of alternatives, and through a correlation coefficient, represent the conflicts between the opposing objective functions.
A normalised decision matrix A_{mxn} (m is the number of Pareto points, n the number of objective functions) is created. Each element of the matrix A, a_{ij}, is calculated by comparing it with the Pareto points reaching the maximum and minimum value of the objective functions:

$$a_{ij} = \frac{Pareto_i - Pareto_{min}}{Pareto_{max} - Pareto_{min}} \tag{6.1}$$

Then, the average value of the elements of A, $\bar{a}$, and the Standard deviation σ_j is calculated, in regard to each column related to each objective function. With these it it possible to calculate the matrix of the correlation coefficients R_{nxn}, where its elements r_{ij} are defined as:

$$r_{ij} = \frac{\sum_{i=1}^{m}(a_{ip} - \bar{a}_i)/(a_{ij} - \bar{a}_j)}{\sqrt{\sum_{i=1}^{m}\left(a_{ip} - \bar{a}_p\right)^2} \cdot \sqrt{\sum_{i=1}^{m}\left(a_{ij} - \bar{a}_j\right)^2}} \qquad p, j = 1 : n \tag{6.2}$$

Finally the weighted normalised decision matrix V_{mxn} is calculated by means of the weight of the objectives vector w:

$$w_j = \frac{\sigma_j \sum_{i=1}^{n}(1 - r_{ij})}{\sum_{j=1}^{m}\left(\sigma_j \sum_{i=1}^{n}(1 - r_{ij})\right)} \tag{6.3}$$

$$V = A \cdot w \tag{6.4}$$

6.3 Ranking Algorithm: TOPSIS

The Technique for Order Preference by Similarity to Ideal Solution (TOPSIS) algorithm is the last of one in the OS, and it is used to determine the best among the weighted solutions obtained through NSGA-II and CRITIC. This method compares each weighted element of the matrix V, with the best z_j^+ and worst z_j^+ performing elements for each objective function. Then, it calculates the distance of each solution to the ideal S_i^+ and to the worst one S_i^-, and finds the closeness C_i of each solution to the optimal one:

$$z_j^+ = min(v_{ij}) \tag{6.5}$$

$$z_j^- = max(v_{ij}) \tag{6.6}$$

$$S_i^+ = \sqrt{\sum_{j=1}^{n} \left(v_{ij} - z_j^+\right)^2} \tag{6.7}$$

$$S_i^- = \sqrt{\sum_{j=1}^{n} \left(v_{ij} - z_j^-\right)^2} \tag{6.8}$$

$$C_i = \frac{S_i^-}{S_i^+ + S_i^-} \tag{6.9}$$

Finally, the solutions are ranked from the closest to the most distant solution to the optimal one, terminating the decision process.

7

Results

The main objective of this project is to find an efficient way to size the hydrogen producing system, and an energy storage system connected to it. Even though similar cases have been studied in the literature, they differ at a point that the same strategies adopted there, do not fit the system here proposed. Therefore, not knowing in advance the right approach to use, different combinations of objective functions from *Chapter 5* have been tried, in order to find the most suitable ones to adopt during the sizing phase. The same analysis and simulations, have been carried for both the control systems described in *Chapter 4*, and for the two scenarios, current and 2030 efficiency, related to the electrolyzers. Finally, the results obtained are analysed in *Chapter 8*.
The different combination of optimisation functions, the sizing strategies, that have been tried are the following:

- CAPEX - LCOH
- CAPEX - LCOH - EDP
- EDP - LCOH
- Conversion CAPEX - Conversion LCOH
- Conversion CAPEX - Conversion LCOH - EDP
- EDP - Conversion LCOH
- BCR - EDP

- BCR - H_2

7.1 Benchmark: LCOH

At the beginning, a set of counterposed functions is not evaluated, but rather a single configuration is found that minimises the LCOH. This one will be used later as a benchmark to evaluate how the other strategies perform, with the different parameters optimised, in relation to that configuration. The configurations obtained have been included in **[Tab.7.1]**. Two things can already be noticed: *System A* nearly neglects the usage of an ESS, and that at the same efficiency scenario, the LCOH is always lower in *System B*.

	Electrolyzers	BSF	LCOH [€/kg]
System A - Current efficiency	194	1	3,56
System A - 2030 efficiency	193	8	2,66
System B - Current efficiency	206	44	3,36
System B - 2030 efficiency	206	43	2,52

Table 7.1: Configurations in the LCOH minimisation case

7.2 CAPEX vs LCOH

The first idea is to try to minimise both the LCOH and the Capital expenditure of the entire project (Wind farm, Hydrogen system, Energy storage system), in order to have a cost of hydrogen that is kept low, but at the same time, avoiding to oversize the hydrogen system, increasing the capital necessary to build it, in an excessive way **[Tab.7.2] [Tab.7.3]**.
The problem with this approach is that the solutions found as optimal by the CRITIC and TOPSIS algorithms, contain values of the LCOH evidently inconvenient for the project, being the installed electrolyzer power insufficient to have an acceptable production of hydrogen. On the other hand, the saving on the CAPEX achieved is very limited.

The OS in all the scenario limits the BSF to 1, which is the minimum value that is accepted by the code, this means that it would have instead chose 0 if it was possible. The $BSF = 1$ solutions can be considered then as *configurations without an ESS*. In **[Fig.7.1]** are shown the yearly power profiles of the top configurations of *System A* and *System B* for the current electrolyzer efficiency scenario.

System A - Current efficiency				
Rank	Electrolyzers	BSF	CAPEX [M€]	LCOH [€/kg]
1	24	1	995,13	11,30
2	25	1	996,37	10,92
3	23	1	993,89	11,72
4	26	1	997,61	10,56
5	22	1	992,65	12,18

System B - Current efficiency				
Rank	Electrolyzers	BSF	CAPEX [M€]	LCOH [€/kg]
1	75	1	1058,07	4,964
2	74	1	1056,84	5,004
3	76	1	1059,30	4,926
4	73	1	1055,61	5,044
5	77	1	1060,53	4,889

Table 7.2: Configurations in the CAPEX-LCOH optimisation case for the current efficiency scenario

System A - Current efficiency				
Rank	Electrolyzers	BSF	CAPEX [M€]	LCOH [€/kg]
1	24	1	995,13	8,404
2	25	1	996,37	8,117
3	23	1	993,89	8,717
4	26	1	997,61	7,852
5	22	1	992,65	9,056

System B - Current efficiency				
Rank	Electrolyzers	BSF	CAPEX [M€]	LCOH [€/kg]
1	74	1	1056,84	3,728
2	73	1	1055,61	3,758
3	75	1	1058,07	3,699
4	72	1	1054,38	3,789
5	76	1	1059,30	3,671

Table 7.3: Configurations in the CAPEX-LCOH optimisation case for the 2030 efficiency scenario

Even though System B performs slightly better having a higher installed electrolyzer capacity, these configurations are both highly inefficient, with most of the produced power dumped.

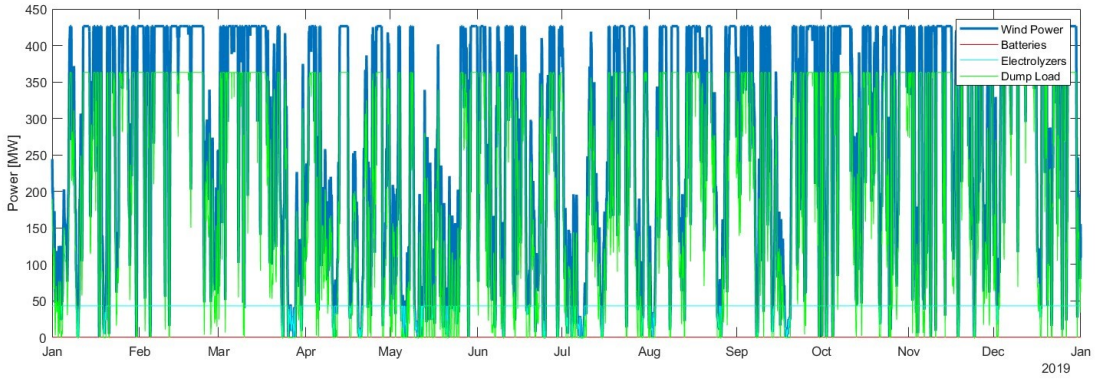

(a) System A - Current efficiency

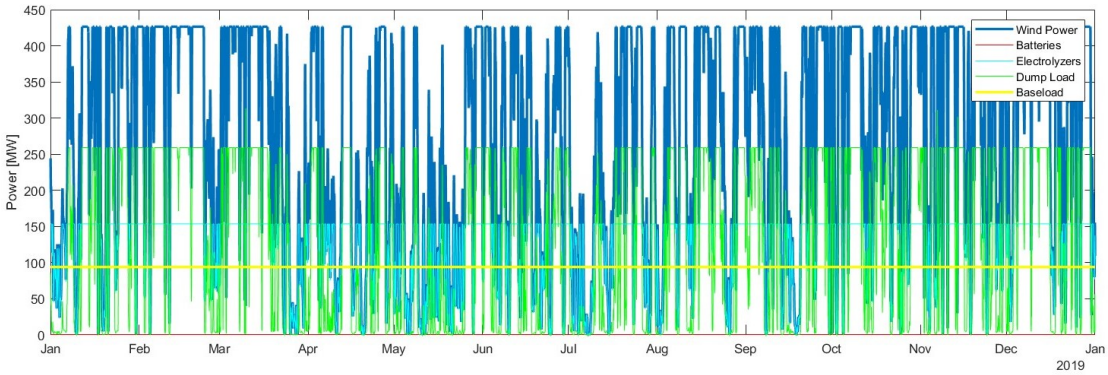

(b) System B - Current efficiency

Figure 7.1: Power profiles for CAPEX-LCOH optimisation

7.3 CAPEX vs LCOH vs EDP

The problem of the previous approach is that by minimising the CAPEX the H2S becomes unable to appropriately exploit the wind resource (thus with a reduction in the hydrogen yield that increases the LCOH). To try to overcome this, it is added a third parameter, the EDP, to reduce the amount of energy that is dumped **[Tab.7.4] [Tab.7.5]**.

Even adding the minimisation of the dumped energy through the EDP objective function, the OS still prefers to maintain the electrolyzer number low, without any mean of energy storage. Also the configurations are nearly the same of the previous case. The power profiles in **[Fig.7.2]** are analogous as well, and the same identical considerations can be drawn.

System A - Current efficiency					
Rank	Electrolyzers	BSF	CAPEX [M€]	LCOH [€/kg]	EDP [%]
1	29	1	1001,33	9,64	74,76
2	30	1	1002,57	9,38	74,11
3	28	1	1000,09	9,93	75,41
4	31	1	1003,81	9,13	73,46
5	27	1	998,85	10,23	76,07

System B - Current efficiency					
Rank	Electrolyzers	BSF	CAPEX [M€]	LCOH [€/kg]	EDP [%]
1	69	1	1050,69	5,219	52,485
2	70	1	1051,92	5,173	51,973
3	68	1	1049,46	5,266	53,000
4	67	1	1048,22	5,314	53,517
5	71	1	1053,15	5,129	51,464

Table 7.4: Configurations in the CAPEX-LCOH-EDP optimisation case for the current efficiency scenario

System A - 2030 efficiency					
Rank	Electrolyzers	BSF	CAPEX [M€]	LCOH [€/kg]	EDP [%]
1	28	1	1000,09	7,38	75,26
2	27	1	998,85	7,61	75,92
3	29	1	1001,33	7,17	74,60
4	26	1	997,61	7,85	76,59
5	30	1	1002,57	6,97	73,95

System B - 2030 efficiency					
Rank	Electrolyzers	BSF	CAPEX [M€]	LCOH [€/kg]	EDP [%]
1	68	1	1049,46	3,92	52,66
2	67	1	1048,22	3,96	53,18
3	66	1	1046,99	4,00	53,71
4	69	1	1050,69	3,89	52,14
5	65	1	1045,76	4,04	54,23

Table 7.5: Configurations in the CAPEX-LCOH-EDP optimisation case for the 2030 efficiency scenario

7.4 EDP vs LCOH

The same choice of optimisation function is reused, but this time it has been tried removing the CAPEX from it, since up til now it has proven itself an inefficient selection parameter. This time, the OS tries to reduce the costs by

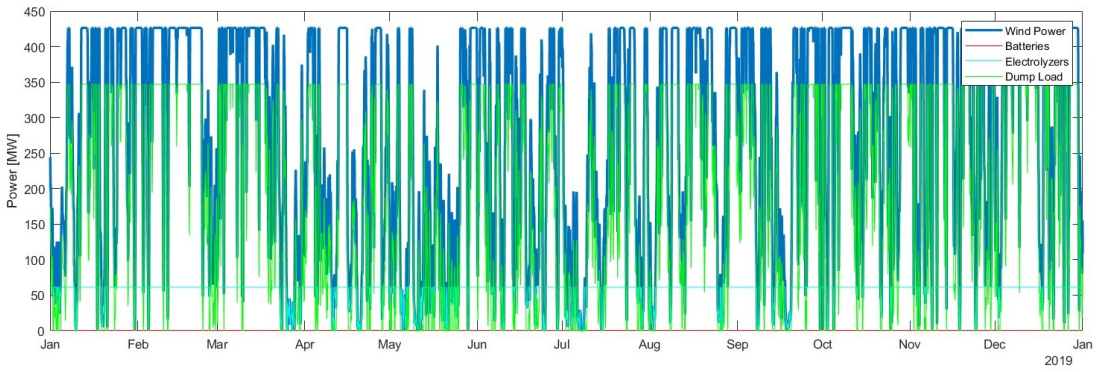

(a) System A - Current efficiency

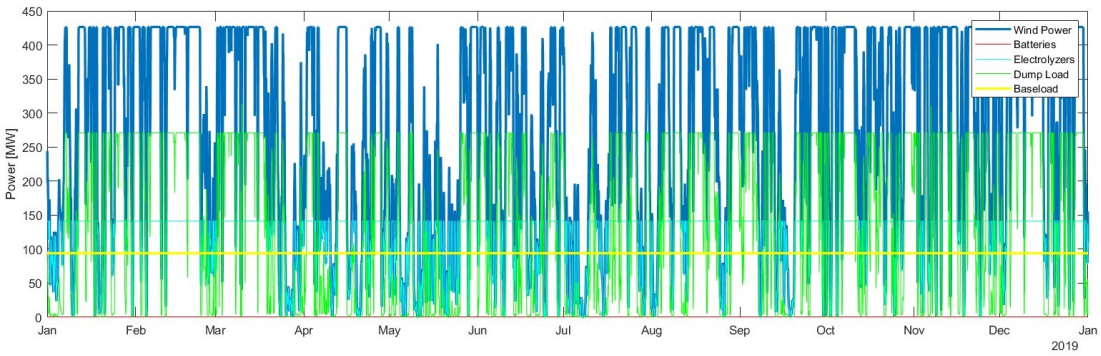

(b) System B - Current efficiency

Figure 7.2: Power profiles for CAPEX-LCOH-EDP optimisation

improving the exploitation of the wind power, until the point the increase in the size of both the ESS and H2S doesn't achieve any further reduction in the total dumped power **[Tab.7.6] [Tab.7.7]**.

The OS selects an H2S capacity that is able to cover completely the power provided by the WF **[Fig.7.3]**. Also, the ESS is used, and its size is relevant (about 80 MW for *System A* and 230 MW for *System B*), even though it is rarely completely filled. The ESS allows to limit the turning OFF of the electrolyzers and stores nearly all the exceeding energy (the EDP values are extremely low).

7.5 Conversion LCOH

The problem concerning the use the CAPEX as an objective function, is that the OS will try to reduce it as much as possible, but being the size of the WF fixed, and because it makes up the greatest part of the final CAPEX

System A - Current efficiency				
Rank	Electrolyzers	BSF	EDP [%]]	LCOH [€/kg]
1	201	166	0,126	3,726
2	201	171	0,122	3,736
3	201	164	0,130	3,724
4	201	177	0,116	3,746
5	201	167	0,125	3,733

System B - Current efficiency				
Rank	Electrolyzers	BSF	EDP [%]	LCOH [€/kg]
1	207	475	0,0390	3,692
2	207	476	0,0389	3,693
3	207	473	0,0391	3,690
4	207	464	0,0398	3,683
5	207	463	0,0399	3,682

Table 7.6: Configurations in the EDP-LCOH optimisation case for the current efficiency scenario

System A - 2030 efficiency				
Rank	Electrolyzers	BSF	EDP [%]]	LCOH [€/kg]
1	200	167	0,1143	2,784
2	200	165	0,1157	2,783
3	200	164	0,1164	2,782
4	200	159	0,1219	2,779
5	200	174	0,1095	2,793

System B - 2030 efficiency				
Rank	Electrolyzers	BSF	EDP [%]	LCOH [€/kg]
1	206	460	0,0394	2,771
2	206	461	0,0393	2,772
3	206	452	0,0400	2,766
4	206	464	0,0391	2,774
5	206	451	0,0401	2,766

Table 7.7: Configurations in the EDP-LCOH optimisation case for the 2030 efficiency scenario

($\sim$ 964 M€), the H2S will be reduced as much as possible, producing very inefficient configurations. It is evident that for a fixed size WF the minimisation of CAPEX as selection criteria has to be avoided, but it is possible to still use it in a modified way that overcomes this issue: the Conversion CAPEX (CCAPEX), that excludes the WF costs from the optimisation process. Thus, the previous

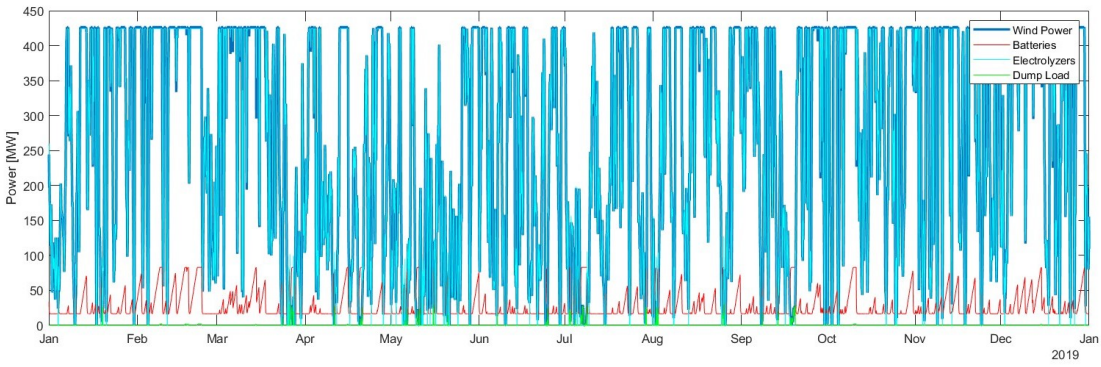

(a) System A - Current efficiency

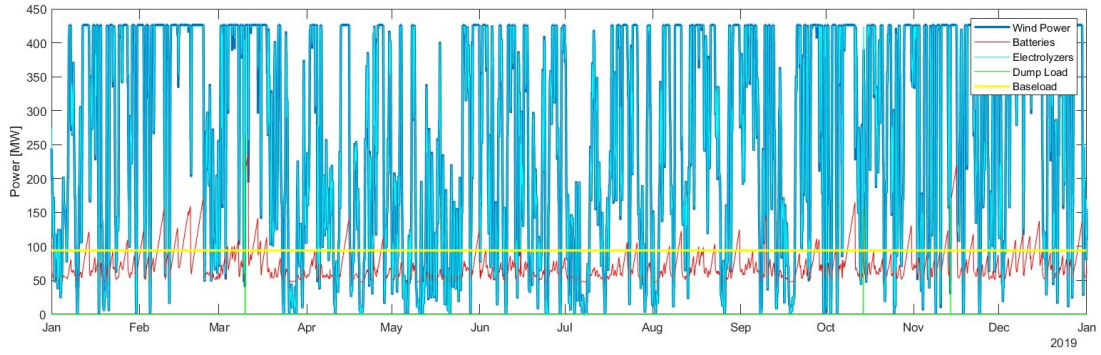

(b) System B - Current efficiency

Figure 7.3: Power profiles for EDP-LCOH optimisation

three function strategies are proposed again, but with the CLCOH instead of the LCOH this time.

7.5.1 CCAPEX vs CLCOH

The first solution remains unsatisfactory, nevertheless the modifications aimed at fixing the CAPEX problem. All the best ranking solutions avoid the use of the ESS with very high LCOH values. Also, for this combination of OFs, there is only one solution instead of a set of Pareto points **[Tab.7.8]**

7.5.2 CCAPEX vs CLCOH vs EDP

Compared to the CAPEX-CLCOH-EDP case, there is an higher number of electrolyzers that increases the production of hydrogen **[Tab.7.9]** **[Tab.7.10]**, however, the ESS is either not contemplated or insufficient, with still an high

	Electrolyzers	BSF	CCAPEX [M€]	CLCOH	LCOH
System A - C.E.	10	1	13,20	1,005	24,80
System A - 2030 E.	10	1	13,21	0,748	18,45
System B - C.E.	47	1	59,12	1,098	6,73
System B - 2030 E.	47	1	59,12	0,818	5,02

Table 7.8: Configurations in the CCAPEX-CLCOH optimisation case

fraction of power lost **[Fig.7.4]**.

System A - Current efficiency					
Rank	Electrolyzers	BSF	CCAPEX [M€]	CLCOH [€/kg]	EDP [%]
1	119	1	147,65	1,331	27,93
2	117	1	145,20	1,322	28,75
3	115	1	142,74	1,313	29,57
4	122	1	151,33	1,348	26,72
5	123	1	152,56	1,353	26,32

System B - Current efficiency					
Rank	Electrolyzers	BSF	CCAPEX [M€]	CLCOH [€/kg]	EDP [%]
1	165	16	207,87	1,431	13,092
2	160	15	201,49	1,417	14,740
3	164	12	205,63	1,428	13,594
4	168	14	211,04	1,440	12,239
5	160	9	199,96	1,416	15,031

Table 7.9: Configurations in the CCAPEX-CLCOH-EDP optimisation case for the current efficiency scenario

7.5.3 EDP vs CLCOH

Compared to the case with the reduction of the full LCOH, this time the size of ESS has shrank (or at have been completely excluded in *System A*) and the size of the H2S have been slightly decreased as well **[Tab.7.11] [Tab.7.12]**.

In **[Fig.7.5]** it can be seen that this time the electrolyzers leave a small portion of the WF power uncovered with a higher amount of dumped energy. Anyway, the dumped energy remains low with an EDP lower than 2%.

System A - 2030 efficiency					
Rank	Electrolyzers	BSF	CCAPEX [M€]	CLCOH [€/kg]	EDP [%]
1	117	1	145,20	0,983	28,36
2	118	1	146,43	0,987	27,95
3	115	1	142,74	0,979	29,18
4	112	1	139,06	0,970	30,44
5	123	1	152,56	1,010	25,93

System B - 2030 efficiency					
Rank	Electrolyzers	BSF	CCAPEX [M€]	CLCOH [€/kg]	EDP [%]
1	164	16	206,64	1,068	12,80
2	164	18	207,15	1,069	12,73
3	157	10	196,54	1,052	15,33
4	171	14	214,71	1,083	10,67
5	158	4	196,24	1,054	15,33

Table 7.10: Configurations in the CCAPEX-CLCOH-EDP optimisation case for the 2030 efficiency scenario

System A - Current efficiency				
Rank	Electrolyzers	BSF	EDP [%]	CLCOH [€/kg]
1	194	1	2,55	1,688
2	193	1	2,82	1,684
3	192	1	3,09	1,680
4	190	1	3,65	1,673
5	195	3	2,26	1,696

System B - Current efficiency				
Rank	Electrolyzers	BSF	EDP [%]	CLCOH [€/kg]
1	199	25	2,917	1,532
2	200	25	2,663	1,535
3	197	32	3,231	1,529
4	196	29	3,573	1,525
5	201	22	2,527	1,537

Table 7.11: Configurations in the EDP-CLCOH optimisation case for the current efficiency scenario

7.6 BCR vs EDP

The last trials have been performed introducing the BCR. The BCR is an economical indicator, and it includes the optimisation of the LCOH in it. This objective function combination tries to improve both the technical and the eco-

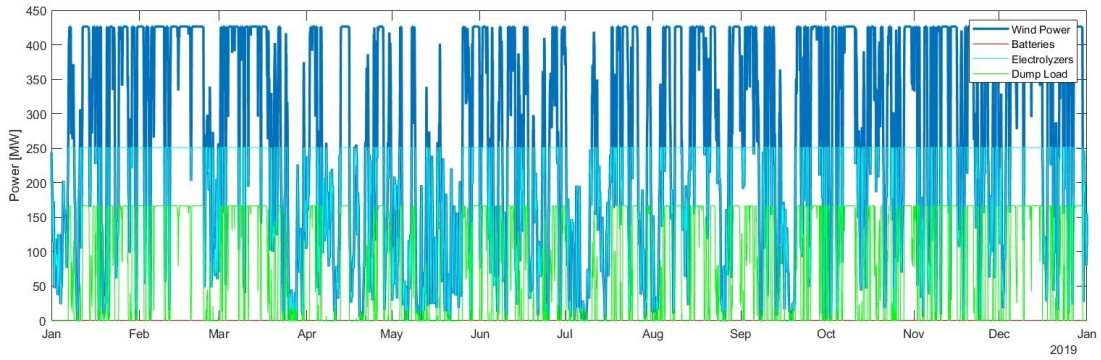

(a) System A - Current efficiency

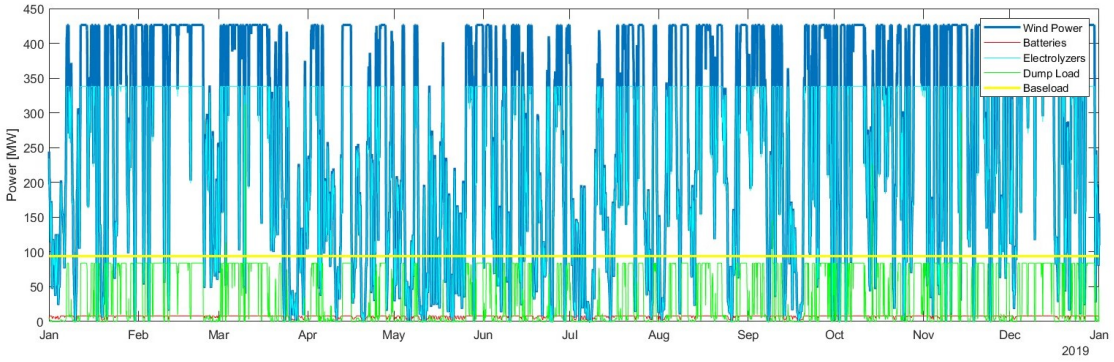

(b) System B - Current efficiency

Figure 7.4: Power profiles for CCAPEX-CLCOH-EDP optimisation

nomical performances of the system **[Tab.7.13] [Tab.7.14]**.

From **[Fig.7.6]** it appears to be similar to the EDP-LCOH case with the electrolyzer capacity at the same level of the WF power after conversion and losses. However, for *System B* the size of the ESS is lower, but the time at which is completely filled is longer. *System A* either avoids, or adopts just few MW of storage.

7.7 BCR vs H_2

Finally in the last trial, the BCR is maximised alongside the quantity of hydrogen produced, to improve both the economical performances and the annual yield of the system **[Tab.7.15] [Tab.7.15]**.

The chosen configurations are fairly similar to those obtained with the EDP, but in *System B* this time the OS opts for an increased number of electrolyzers (and

System A - 2030 efficiency				
Rank	Electrolyzers	BSF	EDP [%]	CLCOH [€/kg]
1	188	1	3,77	1,240
2	189	1	3,49	1,243
3	190	1	3,21	1,246
4	191	1	2,94	1,249
5	191	8	2,88	1,250

System B - 2030 efficiency				
Rank	Electrolyzers	BSF	EDP [%]	CLCOH [€/kg]
1	196	21	3,20	1,140
2	197	26	2,79	1,143
3	198	26	2,52	1,146
4	200	27	1,98	1,151
5	194	19	3,80	1,135

Table 7.12: Configurations in the EDP-CLCOH optimisation case for the 2030 efficiency scenario

System A - Current efficiency				
Rank	Electrolyzers	BSF	BCR	EDP [%]
1	202	1	1,1005	0,470
2	202	2	1,1003	0,463
3	202	4	1,0999	0,452
4	202	6	1,0995	0,443
5	202	8	1,0981	0,435

System B - Current efficiency				
Rank	Electrolyzers	BSF	BCR	EDP [%]
1	209	56	1,1716	0,109
2	209	61	1,1702	0,107
3	209	63	1,1697	0,106
4	209	67	1,1686	0,105
5	209	70	1,1678	0,104

Table 7.13: Configurations in the BCR-EDP optimisation case for the current efficiency scenario

its capacity exceeds the power outup of the WF after losses and transformer), and it slightly reduces the size of the ESS. For *System A* the situation remains nearly identical.

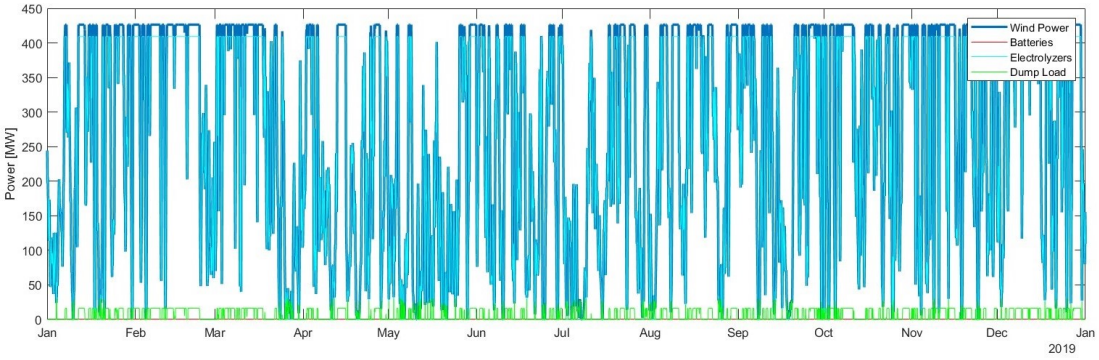

(a) System A - Current efficiency

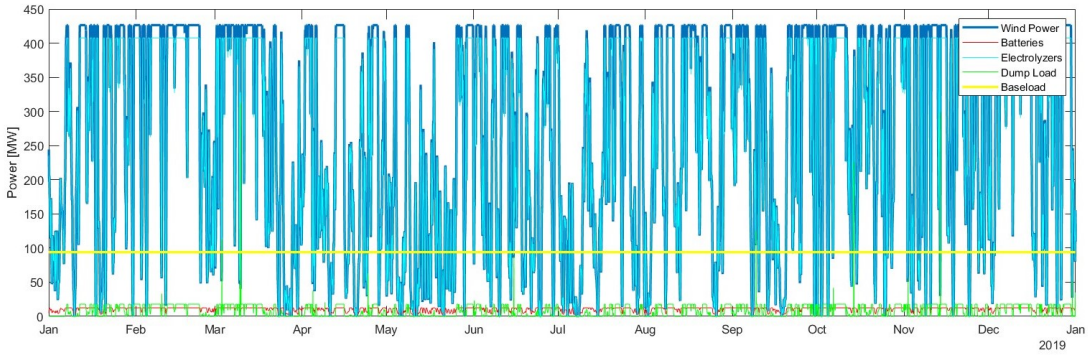

(b) System B - Current efficiency

Figure 7.5: Power profiles for EDP-CLCOH optimisation

System A - 2030 efficiency				
Rank	Electrolyzers	BSF	BCR	EDP [%]
1	201	1	1,4747	0,437
2	201	3	1,4741	0,432
3	201	4	1,4738	0,429
4	201	7	1,4729	0,421
5	201	8	1,4726	0,418

System B - 2030 efficiency				
Rank	Electrolyzers	BSF	BCR	EDP [%]
1	207	67	1,556	0,104
2	207	70	1,555	0,103
3	207	64	1,557	0,105
4	207	72	1,554	0,102
5	207	62	1,558	0,106

Table 7.14: Configurations in the BCR-EDP optimisation case for the 2030 efficiency scenario

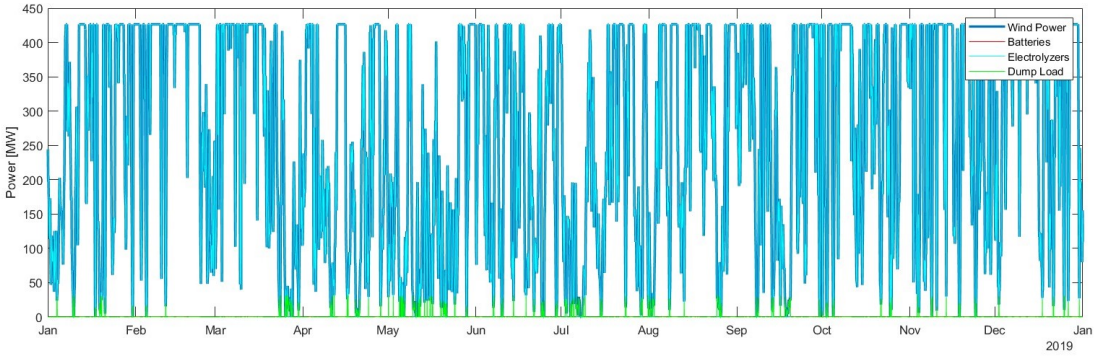

(a) System A - Current efficiency

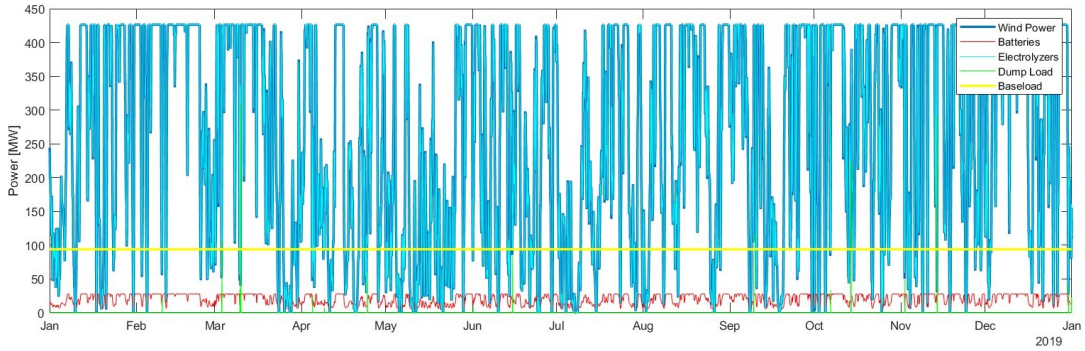

(b) System B - Current efficiency

Figure 7.6: Power profiles for BCR-EDP optimisation

System A - Current efficiency				
Rank	Electrolyzers	BSF	BCR	H_2 [kton]
1	202	3	1,1001	30,878
2	202	1	1,1005	30,874
3	202	6	1,0995	30,882
4	202	7	1,0984	30,883
5	202	9	1,0979	30,885

System B - Current efficiency				
Rank	Electrolyzers	BSF	BCR	H_2 [kton]
1	222	55	1,1522	32,15
2	223	55	1,1507	32,17
3	224	56	1,1490	32,20
4	221	55	1,1538	32,12
5	222	58	1,1516	32,15

Table 7.15: Configurations in the BCR-H2 optimisation case for the current efficiency scenario

System A - 2030 efficiency				
Rank	Electrolyzers	BSF	BCR	H_2 [kton]
1	201	1	1,4747	41,205
2	201	3	1,4741	41,207
3	201	7	1,4729	41,211
4	201	8	1,4726	41,212
5	201	9	1,4711	41,213

System B - 2030 efficiency				
Rank	Electrolyzers	BSF	BCR	H_2 [kton]
1	221	46	1,531	42,4966
2	222	46	1,529	42,519
3	220	46	1,533	42,472
4	223	46	1,526	42,541
5	222	47	1,528	42,520

Table 7.16: Configurations in the BCR-H2 optimisation case for the 2030 efficiency scenario

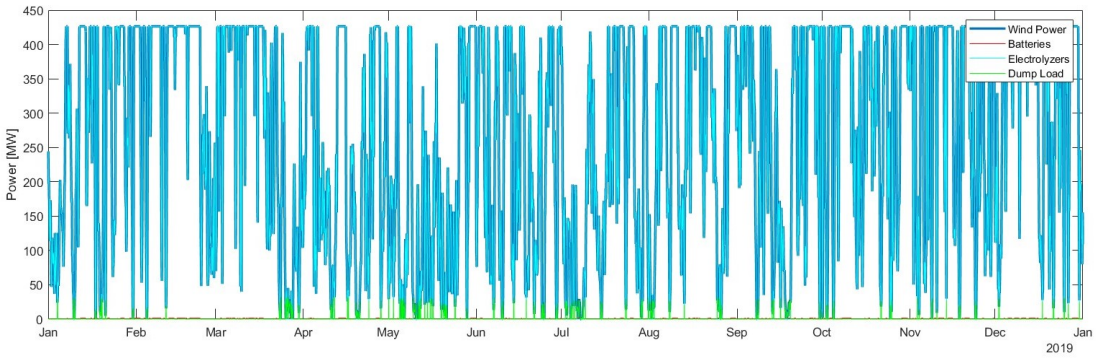

(a) System A - Current efficiency

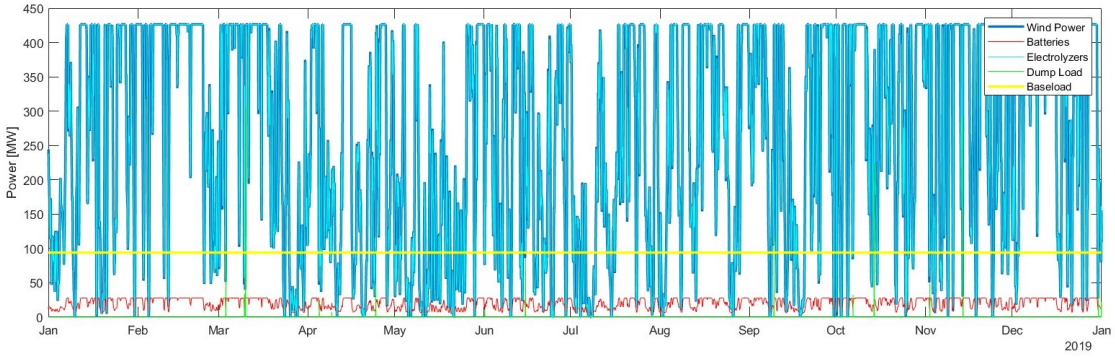

(b) System B - Current efficiency

Figure 7.7: Power profiles for BCR-H2 optimisation

8

Analysis

After that all the simulations have been performed it is necessary to compare all of them through the use of other parameters, because, even though some preliminary considerations can be drawn just by looking at the first results and at the power profiles, it is not immediately clear which are the best choices of objective function combinations (with the exception of the cases that involved the CAPEX or the CCAPEX-CLCOH that are evidently not suitable already at a first glance). The results for each strategy are summarised in **[Tab.8.1] [Tab.8.2] [Tab.8.3] [Tab.8.4]**, where have been added all the parameters evaluated in the analysis, and not only those optimised in each simulation.

	Electrolyzers	BSF	H_2[kton]	BCR	EDP[%]	LCOH [€/kg]	CAPEX [M€]	OPEX [M€]	DECEX [M€]
LCOH	194	1	30,20	1,1056	2,54	3,57	1204,04	101,99	52,88
CAPEX vs LCOH	24	1	5,53	0,3491	78,05	11,30	995,13	36,89	48,80
CAPEX vs LCOH vs EDP	29	1	6,61	0,4093	74,76	9,64	1001,33	38,56	48,92
EDP vs LCOH	201	166	30,94	1,0591	0,11	3,73	1254,58	111,72	53,05
CCAPEX vs CLCOH	10	1	2,39	0,1591	87,69	24,81	977,67	32,24	48,46
CCAPEX vs CLCOH vs EDP	119	1	21,91	1,0056	27,93	3,92	1112,12	69,96	51,08
EDP vs CLCOH	194	1	30,20	1,1056	2,54	3,57	1204,04	101,99	52,88
BCR vs EDP	202	1	30,87	1,1005	0,47	3,59	1213,83	106,50	53,07
BCR vs H2	202	3	30,88	1,1001	0,46	3,59	1214,34	106,55	53,07

Table 8.1: Solutions of System A in Current efficiency scenario

	Electrolyzers	BSF	H_2[kton]	BCR	EDP[%]	LCOH [€/kg]	CAPEX [M€]	OPEX [M€]	DECEX[M€]
LCOH	193	8	40,37	1,4818	2,33	2,66	1204,59	101,49	52,86
CAPEX vs LCOH	24	1	7,44	0,4695	77,92	8,40	995,13	36,83	48,80
CAPEX vs LCOH vs EDP	28	1	8,60	0,5347	75,26	7,38	1000,09	38,16	48,90
EDP vs LCOH	200	167	41,29	1,4107	0,11	2,80	1253,61	112,18	53,02
CCAPEX vs CLCOH	10	1	3,21	0,2139	87,63	18,45	977,67	32,24	48,46
CCAPEX vs CLCOH vs EDP	117	1	29,03	1,3422	28,36	2,94	1109,66	69,08	51,03
EDP vs CLCOH	188	1	39,74	1,4780	3,77	2,67	1196,69	99,58	52,74
BCR vs EDP	201	1	41,20	1,4747	0,44	2,68	1212,61	105,78	53,05
BCR vs H2	201	1	41,20	1,4747	0,44	2,68	1212,61	105,78	53,05

Table 8.2: Solutions of System A in 2030 efficiency scenario

	Electrolyzers	BSF	H_2[ton]	BCR	EDP[%]	LCOH [€/kg]	CAPEX [M€]	OPEX [M€]	DECEX [M€]
LCOH	206	44	31,54	1,1731	0,72	3,36	1229,67	97,17	53,17
CAPEX vs LCOH	75	1	14,99	0,7950	49,46	4,96	1058,07	53,39	50,02
CAPEX vs LCOH vs EDP	69	1	13,99	0,7562	52,49	5,22	1050,69	51,44	49,88
EDP vs LCOH	207	475	31,74	1,0689	0,04	3,69	1340,52	108,94	53,19
CCAPEX vs CLCOH	47	1	10,07	0,5856	64,43	6,74	1023,58	44,28	49,35
CCAPEX vs CLCOH vs EDP	165	16	27,25	1,1221	13,09	3,52	1172,33	83,08	52,18
EDP vs CLCOH	199	25	30,78	1,1683	2,92	3,38	1216,27	94,38	53,00
BCR vs EDP	209	56	31,80	1,1716	0,11	3,37	1236,39	98,47	53,24
BCR vs H2	222	55	32,15	1,1522	0,13	3,42	1252,05	102,67	53,55

Table 8.3: Solutions of System B in Current efficiency scenario

	Electrolyzers	BSF	H_2[kton]	BCR	EDP[%]	LCOH [€/kg]	CAPEX [M€]	OPEX [M€]	DECEX [M€]
LCOH	206	43	42,02	1,5646	0,27	2,52	1229,41	96,97	53,17
CAPEX vs LCOH	74	1	19,90	1,0585	49,59	3,73	1056,84	53,06	50,00
CAPEX vs LCOH vs EDP	68	1	18,55	1,0058	52,66	3,92	1049,46	51,11	49,86
EDP vs LCOH	206	460	42,09	1,4241	0,04	2,77	1335,48	108,39	53,17
CCAPEX vs CLCOH	47	1	13,51	0,7857	64,18	5,02	1023,58	44,28	49,35
CCAPEX vs CLCOH vs EDP	164	16	36,30	1,4985	12,80	2,63	1171,11	82,75	52,16
EDP vs CLCOH	196	21	40,68	1,5557	3,20	2,54	1211,57	93,30	52,93
BCR vs EDP	207	67	42,11	1,5559	0,10	2,54	1236,74	97,95	53,19
BCR vs H2	221	46	42,50	1,5310	0,11	2,58	1248,54	101,92	53,53

Table 8.4: Solutions of System B in 2030 efficiency scenario

8.1 Comparisons

Firstly, all the configurations are compared with the LCOH minimisation case, that is used as a benchmark through the H_2 production, BCR, LCOH and EDP parameters. The comparisons represent an improvement from the reference case when they come with a positive index. When an increase in the parameter in the i configuration is beneficial, the Benefit is defined as:

$$Benefit_i = \frac{Value_i - Value_{LCOH}}{Value_{LCOH}} \tag{8.1}$$

otherwise, if it is preferable a decrease:

$$Benefit_i = \frac{Value_{LCOH} - Value_i}{Value_{LCOH}} \tag{8.2}$$

The comparisons are shown in **[Tab.8.5] [Tab.8.6] [Tab.8.7] [Tab.8.8]**.

	H_2	BCR	LCOH	EDP
LCOH	0%	0%	0%	0%
CAPEX vs LCOH	-81,7%	-68,4%	-216,7%	-2967,4%
CAPEX vs LCOH vs EDP	-78,1%	-63,0%	-170,2%	-2837,7%
EDP vs LCOH	2,5%	-4,2%	-4,4%	95,7%
CCAPEX vs CLCOH	-92,1%	-85,6%	-595,0%	-3346,0%
CCAPEX vs CLCOH vs EDP	-27,5%	-9,1%	-10,0%	-997,6%
EDP vs CLCOH	0%	0%	0%	0%
BCR vs EDP	2,2%	-0,5%	-0,5%	81,6%
BCR vs H2	2,3%	-0,5%	-0,5%	82,1%

Table 8.5: System A - Current efficiency comparisons

	H_2	BCR	LCOH	EDP
LCOH	0%	0%	0%	0%
CAPEX vs LCOH	-81,6%	-68,3%	-215,6%	-3248,3%
CAPEX vs LCOH vs EDP	-78,7%	-63,9%	-177,1%	-3133,8%
EDP vs LCOH	2,3%	-4,8%	-5,0%	95,4%
CCAPEX vs CLCOH	-92,0%	-85,6%	-592,8%	-3665,4%
CCAPEX vs CLCOH vs EDP	-28,1%	-9,4%	-10,4%	-1118,4%
EDP vs CLCOH	-1,5%	-0,3%	-0,3%	-62,2%
BCR vs EDP	2,1%	-0,5%	-0,5%	81,2%
BCR vs H2	2,1%	-0,5%	-0,5%	81,2%

Table 8.6: System A - 2030 efficiency comparisons

As it was already known, the CAPEX-LCOH, CAPEX-LCOH-EDP and CCAPEX-CLCOH are the worst optimisation strategy and perform badly in each parameters. This optimisation strategies can be therefore avoided. CCAPEX-CLCOH-EDP and EDP-CLCOH are also worst than the LCOH case for each parameter, but the percentage variation is not as great as the before mentioned cases. Anyway, their main disadvantage is the bigger EDP with a relevant amount of power

	H_2	BCR	LCOH	EDP
LCOH	0%	0%	0%	0%
CAPEX vs LCOH	-52,5%	-32,2%	-47,6%	-6722,8%
CAPEX vs LCOH vs EDP	-55,6%	-35,5%	-55,1%	-7140,7%
EDP vs LCOH	0,6%	-8,9%	-9,7%	94,6%
CCAPEX vs CLCOH	-68,1%	-50,1%	-100,3%	-8788,9%
CCAPEX vs CLCOH vs EDP	-13,6%	-4,3%	-4,5%	-1706,1%
EDP vs CLCOH	-2,4%	-0,4%	-0,4%	-302,4%
BCR vs EDP	0,8%	-0,1%	-0,1%	84,9%
BCR vs H2	1,9%	-1,8%	-1,8%	82,6%

Table 8.7: System B - Current efficiency comparisons

	H_2	BCR	LCOH	EDP
LCOH	0%	0%	0%	0%
CAPEX vs LCOH	-52,6%	-32,3%	-47,8%	-17943,2%
CAPEX vs LCOH vs EDP	-55,8%	-35,7%	-55,6%	-19060,5%
EDP vs LCOH	0,2%	-9,0%	-9,9%	85,7%
CCAPEX vs CLCOH	-67,8%	-49,8%	-99,1%	-23254,0%
CCAPEX vs CLCOH vs EDP	-13,6%	-4,2%	-4,4%	-4556,7%
EDP vs CLCOH	-3,2%	-0,6%	-0,6%	-1063,0%
BCR vs EDP	0,2%	-0,6%	-0,6%	62,1%
BCR vs H2	1,1%	-2,2%	-2,2%	59,1%

Table 8.8: System B - 2030 efficiency comparisons

dumped. The other three, EDP-LCOH, BCR-EDP and BCR-H2, improve the utilisation of energy reducing the wasted power (smaller EDP) and as a consequence the amount of produced hydrogen is higher (bigger H_2). These three are then the best choices, but this initial analysis is not sufficient to clearly determine which one is better.

To gain a better understanding of how these configurations perform, and how they are in relation to each other, two other indicators are used, the Discounted Payback time, the time needed for the investment to become profitable, and the Discounted ROI, the Return On Investment, that gives information on how much of net profit is gained for each unit of capital invested:

$$Costs_i = \frac{OPEX_i}{(1+r)^i} \tag{8.3}$$

$$Costs_0 = CAPEX + DECEX \tag{8.4}$$

$$Cash\,Flows_i = \frac{H_{2_i} \cdot p_{H_2}}{(1+r)^i} \tag{8.5}$$

$$Profits_i = Cash\,Flows_i - Costs_i \tag{8.6}$$

$$Cumulated\,Profits_i = Profits_i + Profits_{i-1} \tag{8.7}$$

$$Payback\,Time = year_{i^+} + \frac{-Cumulated\,Profits_{i^+-1}}{Profits_{i^+}} \tag{8.8}$$

$$ROI = \frac{\sum_{n=1}^{life} Profits_i}{\sum_{n=0}^{life} Costs_i} \tag{8.9}$$

where i^+ is the year when the $Cumulated\,Profits$ become positive. The value $life$ is the total project lifetime and it is 25 years, the discount rate r is 5% and in this case the price at which the hydrogen is sold p_{H_2} is supposed to be the same for all the project lifetime and equal to 7€. The results are shown in **[Tab.8.9] [Tab.8.10] [Tab.8.11] [Tab.8.12]**.

	LCOH [€/kg]	Payback Time [years]	ROI [%]
LCOH	3,569	17,52	10,56
CAPEX vs LCOH	11,303	\	-65,09
CAPEX vs LCOH vs EDP	9,642	\	-59,07
EDP vs LCOH	3,726	20,02	5,91
CCAPEX vs CLCOH	24,808	\	-84,09
CCAPEX vs CLCOH vs EDP	3,925	24,52	0,56
EDP vs CLCOH	3,569	17,52	10,56
BCR vs EDP	3,586	17,68	10,05
BCR vs H2	3,587	17,70	10,01

Table 8.9: Economical performances of System A - Current efficiency scenario with fixed selling price

As it was foreseeable, the combinations CAPEX-LCOH, CAPEX-LCOH-EDP and CCAPEX-CLCOH never reach profitability during the project lifetime and their ROI is always negative (the only exception is for the first two for *System B* in the 2030 efficiency scenario, however they become profitable too late). EDP-LCOH and CCAPEX-CLCOH-EDP even being profitable perform worse

	LCOH [€/kg]	Payback Time [years]	ROI [%]
LCOH	2,663	8,74	48,18
CAPEX vs LCOH	8,405	\	-53,05
CAPEX vs LCOH vs EDP	7,381	\	-46,53
EDP vs LCOH	2,797	9,46	41,07
CCAPEX vs CLCOH	18,451	\	-78,61
CCAPEX vs CLCOH vs EDP	2,940	11,62	34,22
EDP vs CLCOH	2,670	8,82	47,80
BCR vs EDP	2,676	8,72	47,47
BCR vs H2	2,676	8,72	47,47

Table 8.10: Economical performances of System A - 2030 efficiency scenario with fixed selling price

	LCOH [€/kg]	Payback Time [years]	ROI [%]
LCOH	3,364	15,00	17,31
CAPEX vs LCOH	4,964	\	-20,50
CAPEX vs LCOH vs EDP	5,219	\	-24,38
EDP vs LCOH	3,692	19,60	6,89
CCAPEX vs CLCOH	6,739	\	-41,44
CCAPEX vs CLCOH vs EDP	3,517	17,25	12,21
EDP vs CLCOH	3,378	15,22	16,83
BCR vs EDP	3,368	15,03	17,16
BCR vs H2	3,425	15,63	15,22

Table 8.11: Economical performances of System B - Current efficiency scenario with fixed selling price

	LCOH [€/kg]	Payback Time [years]	ROI [%]
LCOH	2,522	8,07	56,46
CAPEX vs LCOH	3,728	21,04	5,85
CAPEX vs LCOH vs EDP	3,924	24,55	0,58
EDP vs LCOH	2,771	9,57	42,41
CCAPEX vs CLCOH	5,023	\	-21,43
CCAPEX vs CLCOH vs EDP	2,633	9,05	49,85
EDP vs CLCOH	2,537	8,22	55,57
BCR vs EDP	2,536	8,14	55,59
BCR vs H2	2,578	8,30	53,10

Table 8.12: Economical performances of System B - 2030 efficiency scenario with fixed selling price

than the other remaining solutions (in fact, excluding the worst scoring combinations, they have the highest LCOH values). In each scenario and control

system, the LCOH minimisation solution always achieves the lowest payback times and the highest ROI. However, the other three, EDP-CLCOH, BCR-EDP and BCR-H2 reach values really close to it. Comparing these three it can be seen that they behave differently according to the control system chosen: in *System A*, EDP-CLOCH is always the one with highest ROI of the three (also in the Current efficiency scenario its values are the same of the LCOH case, having in fact the same ESS and electrolyzer capacity), while in *System B* it is second to the BCR-EDP combination.
A last analysis is performed by varying the price of the hydrogen p_{H_2}. It is supposed to not be always constant, but to decrease during the time, hypothesising that with an increase in the number of hydrogen producing systems in the future the costs will be continuously reduced, with the market price of hydrogen being reduced over the time. Thus, the same performances are recalculated, with p_{H_2} decreasing each 5 years: €7 (year 1 to year 5), €6 (year 6 to year 10), €5 (year 11 to year 15), €4 (year 16 to year 20) and €3,5 (year 21 to year 25). The results are shown in **[Tab.8.13] [Tab.8.14] [Tab.8.15] [Tab.8.16]**.

	LCOH [€/kg]	Payback Time [years]	ROI [%]
LCOH	3,57	\	-12,60
CAPEX vs LCOH	11,30	\	-72,40
CAPEX vs LCOH vs EDP	9,64	\	-67,65
EDP vs LCOH	3,73	\	-16,27
CAPEX vs Simple LCOH	24,81	\	-87,42
CAPEX vs Simple LCOH vs EDP	3,92	\	-20,51
EDP vs Simple LCOH	3,57	\	-12,60
BCR vs EDP	3,59	\	-13,01
BCR vs H2	3,59	\	-13,04

Table 8.13: Economical performances of System A - Current efficiency scenario with varying selling price

In all the simulations performed with the current efficiency load-efficiency curve, the profitability is never reached if there is a reduction in the price of hydrogen, and so on the profits. A different result is seen with the 2030 efficiency case, with all the combinations, excluding the worst three, reaching it. The considerations for the combinations of objective functions remain the same as it was said before. The LCOH minimisation gives the best configuration, however, there are two alternatives that achieve similar economical results with two additional advantages: EDP-CLCOH can be convenient if it is preferred

	LCOH [€/kg]	Payback Time [years]	ROI [%]
LCOH	2,66	9,95	17,14
CAPEX vs LCOH	8,40	\	-62,88
CAPEX vs LCOH vs EDP	7,38	\	-57,73
EDP vs LCOH	2,80	11,47	11,52
CAPEX vs Simple LCOH	18,45	\	-83,09
CAPEX vs Simple LCOH vs EDP	2,94	15,57	6,10
EDP vs Simple LCOH	2,67	10,06	16,84
BCR vs EDP	2,68	9,94	16,58
BCR vs H2	2,68	9,94	16,58

Table 8.14: Economical performances of System A - 2030 efficiency scenario with varying selling price

	LCOH [€/kg]	Payback Time [years]	ROI [%]
LCOH	3,36	\	-7,27
CAPEX vs LCOH	4,96	\	-37,16
CAPEX vs LCOH vs EDP	5,22	\	-40,22
EDP vs LCOH	3,69	\	-15,50
CAPEX vs Simple LCOH	6,74	\	-53,71
CAPEX vs Simple LCOH vs EDP	3,52	\	-11,29
EDP vs Simple LCOH	3,38	\	-7,65
BCR vs EDP	3,37	\	-7,39
BCR vs H2	3,42	\	-8,91

Table 8.15: Economical performances of System B - Current efficiency scenario with varying selling price

	LCOH [€/kg]	Payback Time [years]	ROI [%]
LCOH	2,52	8,98	23,69
CAPEX vs LCOH	3,73	\	-16,33
CAPEX vs LCOH vs EDP	3,92	\	-20,49
EDP vs LCOH	2,77	11,59	12,58
CAPEX vs Simple LCOH	5,02	\	-37,89
CAPEX vs Simple LCOH vs EDP	2,63	10,41	18,46
EDP vs Simple LCOH	2,54	9,18	22,98
BCR vs EDP	2,54	9,08	23,00
BCR vs H2	2,58	9,32	21,03

Table 8.16: Economical performances of System B - 2030 efficiency scenario with varying selling price

to slightly decrease the size of the system, to reduce the space occupied in the offshore platforms. Alternatively, with BCR-EDP the size is increased a little

bit and it can be a choice to be considered if it is wanted to increase a bit the hydrogen yield and have a further improvement in the utilisation of energy.
The performance of the configuration for *System B* in 2030 efficiency chosen by the LCOH minimisation case are presented in the figures here below, that show the power profiles **[Fig.8.1]**, how the ESS works **[Fig.8.2]**, and the hydrogen production in relation to the WF production **[Fig.8.3]**

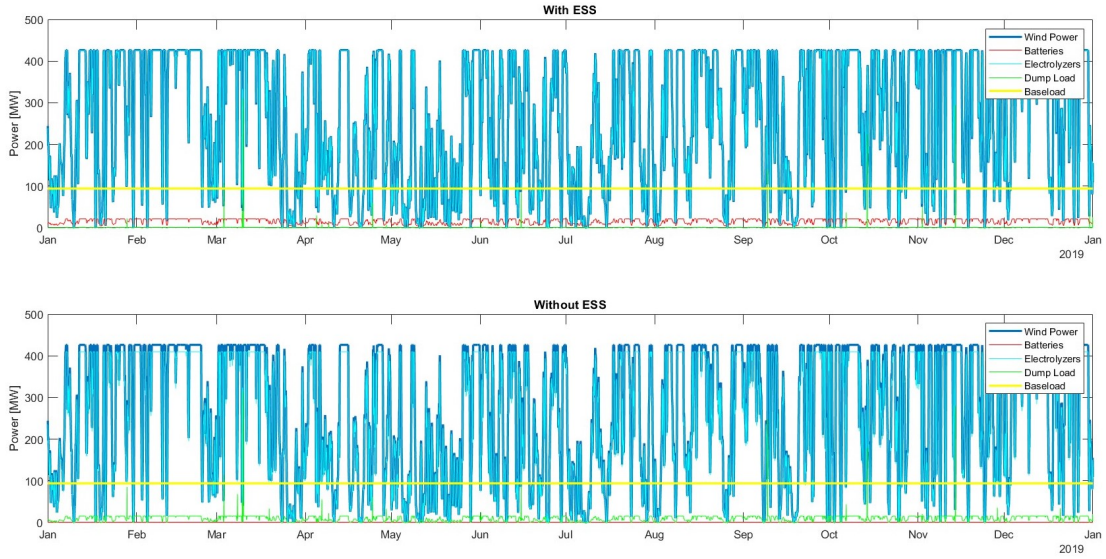

Figure 8.1: LCOH) System B - 2030 Efficiency with and without the ESS

8.2 Battery Analysis

Finally, the role of the batteries in the system is evaluated to understand what is their contribution to the hydrogen production, and their optimal size in the system in relation to the electrolyzer size and their price.
A comparison of the size of the ESS for every scenario and in the main strategies can be seen in **[Fig.8.4]** and in **[Tab.8.17]** **[Tab.8.18]**, where $ESS_{\%}$ indicates the size of the ESS as a percentage of the electrolyzer capacity

As it was said, *System A* avoids the use of an energy storage except in the EDP-LCOH case. Differently, in *System B*, in the best sizing strategies the size of the ESS ranges between ~ 3% and ~ 6% (with ~ 8% in the case of BCR-EDP in the 2030 scenario), with the benchmark positioned at ~ 5%. Therefore, it appears that an ESS is needed, but its size should not be too high, as its purpose is mainly to optimise the ON/OFF cycles of the electrolyzers, and it is better

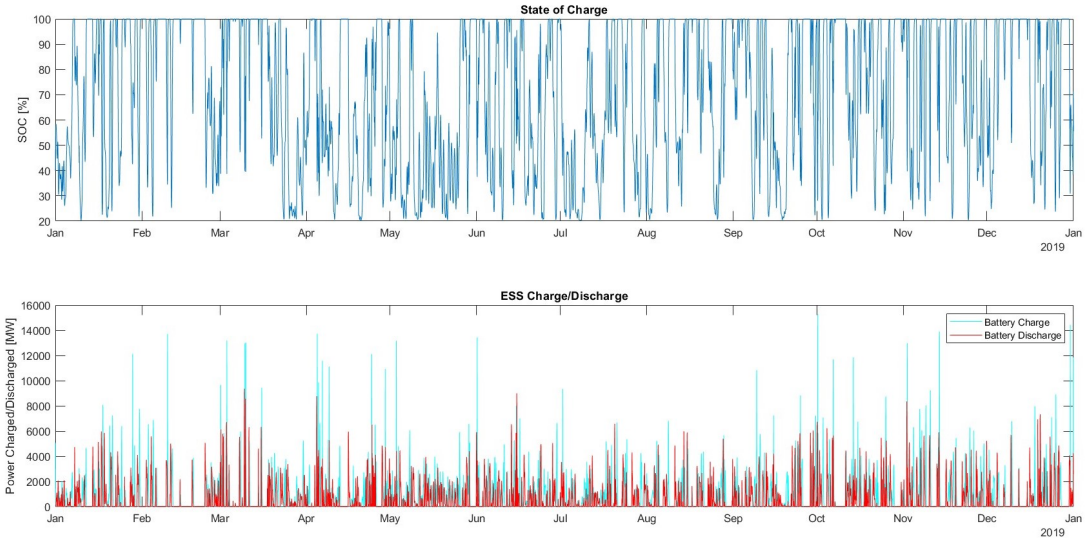

Figure 8.2: LCOH) System B - 2030 Efficiency: SOC, charge and discharge of the ESS

System A						
Strategy	Current Efficiency			2030 Efficiency		
	Size El. [MW]	Size ESS [MW]	Size ESS%	Size El. [MW]	Size ESS [MW]	Size ESS%
LCOH	388	0,5	0,13	386	4	1,04
EDP vs LCOH	402	83	20,65	400	83,5	20,88
CCAPEX vs CLCOH vs EDP	238	0,5	0,21	234	0,5	0,21
EDP vs CLCOH	388	0,5	0,13	376	0,5	0,13
BCR vs EDP	404	0,5	0,12	402	0,5	0,12
BCR vs H2	404	1,5	0,37	402	0,5	0,12

Table 8.17: Size of ESS and H2S in System A

System B						
Strategy	Current Efficiency			2030 Efficiency		
	Size El. [MW]	Size ESS [MW]	Size ESS%	Size El. [MW]	Size ESS [MW]	Size ESS%
LCOH	412	22	5,34	412	21,5	5,22
EDP vs LCOH	414	237,5	57,37	412	230	55,83
CCAPEX vs CLCOH vs EDP	330	8	2,42	328	8	2,44
EDP vs CLCOH	398	12,5	3,14	392	10,5	2,68
BCR vs EDP	418	28	6,70	414	33,5	8,09
BCR vs H2	444	27,5	6,19	442	23	5,20

Table 8.18: Size of ESS and H2S in System B

to have a great number of electrolyzers instead. In **[Fig.8.5]** are compared the component of the CAPEX of the three main solutions for *System B* in the 2030 scenario, and it can be immediately seen that it is made up mostly by the WF

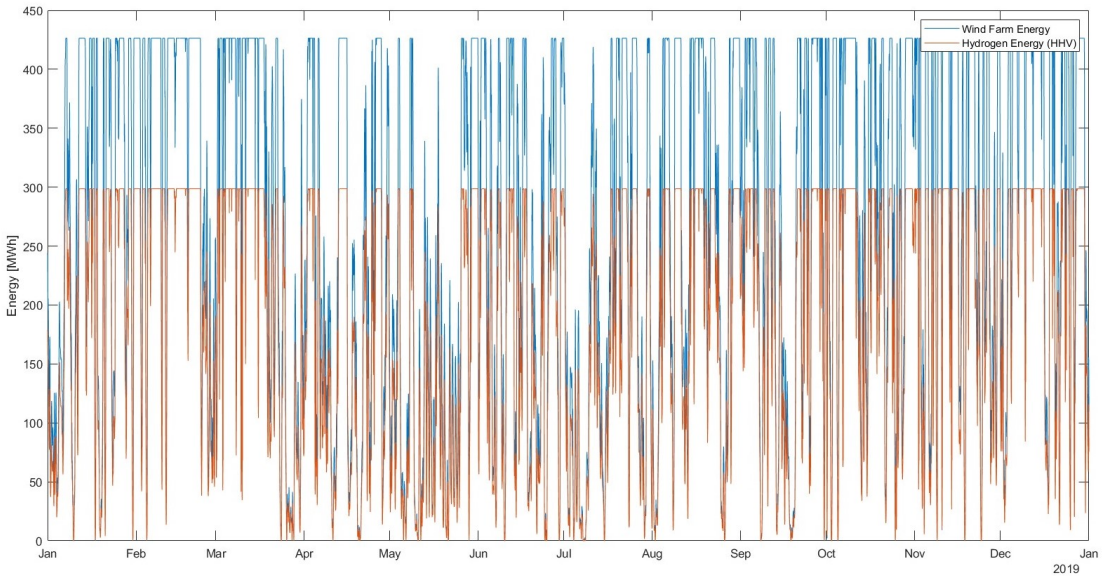

Figure 8.3: LCOH) System B - 2030 Efficiency: energy comparison between the WF and the hydrogen evaluated at the HHV

and the electrolyzers, and the CAPEX of the ESS always remain below the 2% of the total.

The way the costs of the ESS system has been estimated in Chapter 5, is based on the previsions of [39] for 2030, and the OS has optimised its size also according to this.

Let's now suppose that in the near future the price reduction of lithium ion batteries would be stronger than expected. How would the OS size the WtH2 system with these new hypothesis? To answer to this, new simulations have been performed with *System B* in 2030 scenario for LCOH, EDP-CLCOH and BCR-EDP, adding a factor to reduce the CAPEX, the OPEX and the $Cost_{Replace}$ of the ESS by 10%, 20%, 40% and 50%. The results obtained are shown in **[Tab.8.19]**.

The improvements reached, even with an hypothetical 50% decrease in the costs, are negligible. The EDP-CLCOH increases it size and it tends to the LCOH minimisation solution, that just adds 0,5 MW of ESS, and remains constant maintaining always the best performances. It can be then said that the size of the ESS is not strictly dependent on its cost, and that its overall size should not be too high compared to that of the H2S.

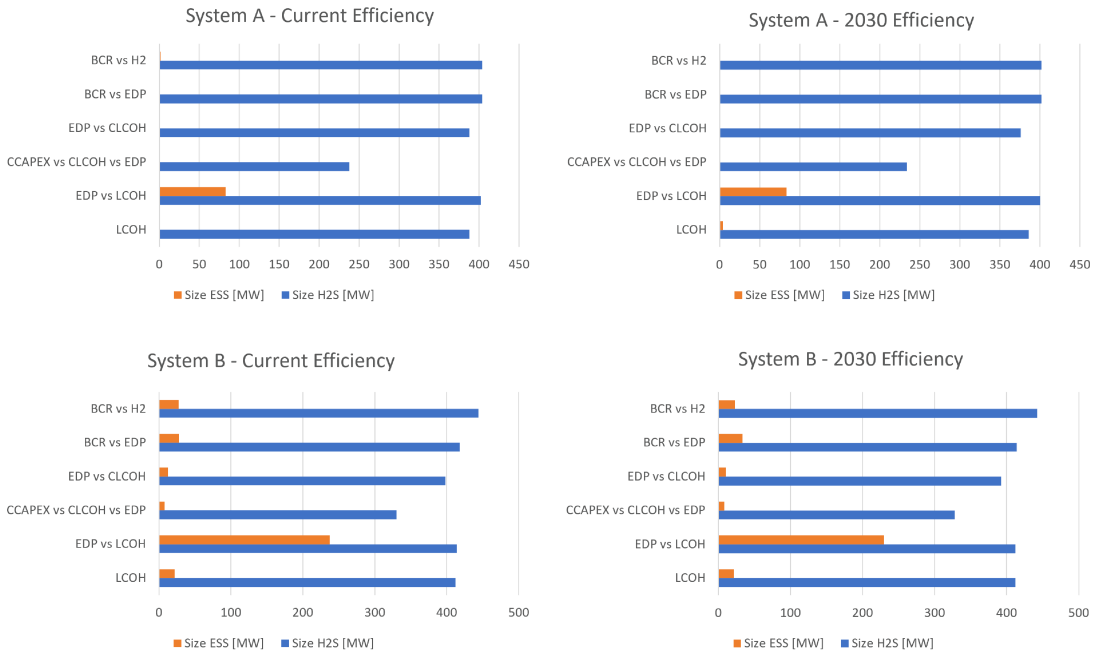

Figure 8.4: Size of ESS and Electrolyzers in every configuration

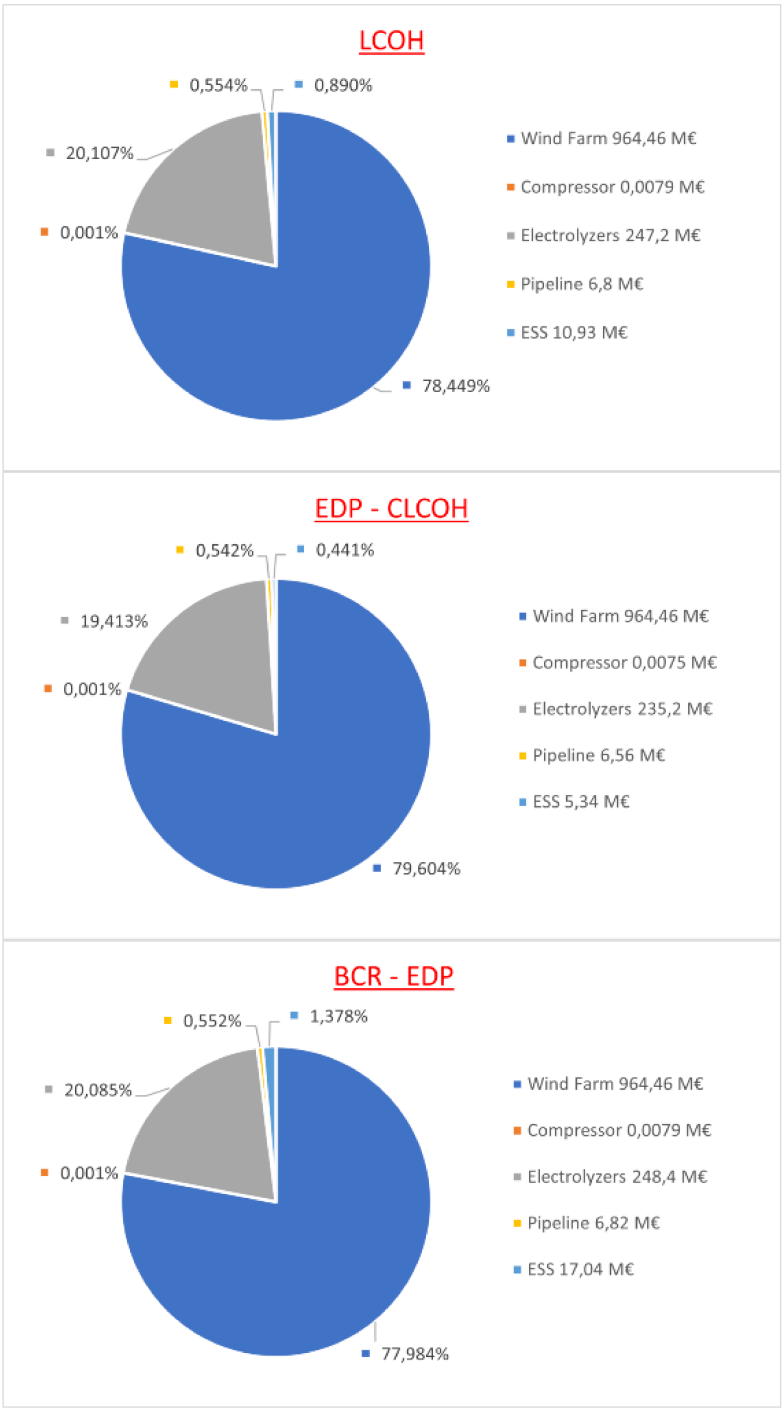

Figure 8.5: CAPEX components of the three main solutions

LCOH Minimisation				
	Electrolyzers	BSF	LCOH	BCR
0% Cost Reduction	206	43	2,522	1,565
10% Cost Reduction	206	44	2,520	1,566
20% Cost Reduction	206	44	2,517	1,568
40% Cost Reduction	206	44	2,512	1,571
50% Cost Reduction	206	44	2,509	1,573

BCR/EDP Optimisation				
	Electrolyzers	BSF	LCOH	BCR
0% Cost Reduction	207	67	2,536	1,5559
10% Cost Reduction	207	78	2,538	1,5548
20% Cost Reduction	207	65	2,527	1,5615
40% Cost Reduction	207	89	2,528	1,5611
50% Cost Reduction	207	104	2,527	1,5617

EDP/CLCOH Optimisation				
	Electrolyzers	BSF	LCOH	BCR
0% Cost Reduction	196	21	2,5366	1,5557
10% Cost Reduction	200	25	2,528	1,5613
20% Cost Reduction	198	29	2,529	1,5605
40% Cost Reduction	199	31	2,523	1,5639
50% Cost Reduction	203	44	2,513	1,5705

Table 8.19: Configurations for reduced battery cost

9 Conclusions

The main goal of this project was to understand which criteria should be used in order to optimally size a Wind-to-Hydrogen system. To do so, a simplified model of the WtH2S has been built inside an Optimisation System, that by mean of algorithms, selected the best configurations of the size of the Electrolyzer and the Energy Storage Systems, based on the chosen combinations of objective functions. Different objective functions have thus been tried to find the best approach to use, and after comparing all of them the following considerations have been drawn, answering the initial questions:

1. **What is the optimal electrolyzer capacity of the Hydrogen System?**

    - To size the system, the minimisation of the LCOH have been found to be the best approach in economical terms, otherwise the two other solutions would be either co-optimising the EDP and the Conversion LCOH, having a smaller size (and therefore smaller occupied space), or the BCR and EDP, with a bigger size with a slightly increased hydrogen yield.
    - The electrolyzers are the main component of the system. It is fundamental that their overall installed capacity meets almost entirely the output power from the wind farm
    - If the efficiencies at 2030 that are foreseen for the electrolyzers are not achieved, the system would risk to not reach profitability if there would be a decrease in the market price of hydrogen during its lifetime.

2. **Would an Energy Storage System beneficial to it? And what would be its size?**

- The battery system is fundamental to help reducing the ON/OFF cycles and to store the energy from the Wind Farm that would be otherwise get lost. However, it is preferable to have an electrolyzer capacity that is close the power output of the WF, while the ESS should be ways more smaller, and it has been found to be between the 2% and the 8% of the electrolyzers total size, with an optimum around 5%.
- The costs of the system are made largely by the Wind Farm (more than 70% of the total) and by the electrolyzer stacks (about 20%). The ESS usually has an impact on the cost lower than the 2%, and it has been seen that even with an hypothetical reduction in price, an increase in the size of the ESS would not give relevant benefits.

3. **What is the best way to control the whole system?**

   - It is better to use a control system that set a constrain to the maximum daily ON/OFF cycles that are allowed for the electrolyzers. This approach has only advantages: it prevents potential damages to the machines, but also it allows to obtain an higher hydrogen yields and better economical performances, in terms of LCOH, Payback Time and Return on Investment.

References

[1] Global Modeling {and} Assimilation Office (GMAO). *Modern-Era Retrospective analysis for Research and Applications, Version 2, inst3_3d_asm_Cp: MERRA-2 3D IAU State, Meteorology Instantaneous 3-hourly (p-coord, 0.625x0.5L42)*. Version version 5.12.4. Greenbelt, MD, USA: Goddard Space Flight Center Distributed Active Archive Center (GSFC DAAC), 2015. URL: https://doi.org/10.5067/VJAFPLI1CSIV (visited on 02/28/2023).

[2] Adam Hayes et al. *Benefit-Cost Ratio (BCR): Definition, Formula, and Example*. Investopedia. Mar. 2022. URL: https://www.investopedia.com/terms/b/bcr.asp (visited on 03/28/2023).

[3] Aliaksei Patonia, Rahmatallah Poudineh. *Cost-competitive green hydrogen: how to lower the cost of electrolysers?* Oxford Institute for Energy Studies. Jan. 2022. URL: https://www.oxfordenergy.org/publications/cost-competitive-green-hydrogen-how-to-lower-the-cost-of-electrolysers/ (visited on 10/18/2022).

[4] Alexandros Arsalis, Panos Papanastasiou, and George E. Georghiou. "A comparative review of lithium-ion battery and regenerative hydrogen fuel cell technologies for integration with photovoltaic applications". In: *Renewable Energy* 191 (May 1, 2022), pp. 943–960. ISSN: 0960-1481. DOI: 10.1016/j.renene.2022.04.075. URL: https://www.sciencedirect.com/science/article/pii/S0960148122005365 (visited on 10/18/2022).

[5] N'guessan S. Attemene et al. "Optimal sizing of a wind, fuel cell, electrolyzer, battery and supercapacitor system for off-grid applications". In: *International Journal of Hydrogen Energy*. 22nd World Hydrogen Energy Conference 45.8 (Feb. 14, 2020), pp. 5512–5525. ISSN: 0360-3199. DOI: 10.1016/j.ijhydene.2019.05.212. URL: https://www.sciencedirect.com/science/article/pii/S0360319919321275 (visited on 10/18/2022).

[6] Thomas Bowen et al. *USAID Grid-Scale Energy Storage Technologies Primer*. NREL/TP-6A20-76097, 1808490, MainId:7155. July 12, 2021, NREL/TP–6A20–76097, 1808490, MainId:7155. DOI: 10.2172/1808490. URL: https://www.osti.gov/servlets/purl/1808490/ (visited on 10/18/2022).

[7] Gonçalo Calado and Rui Castro. "Hydrogen Production from Offshore Wind Parks: Current Situation and Future Perspectives". In: *Applied Sciences* 11.12 (Jan. 2021). Number: 12 Publisher: Multidisciplinary Digital Publishing Institute, p. 5561. ISSN: 2076-3417. DOI: 10.3390/app11125561. URL: https://www.mdpi.com/2076-3417/11/12/5561 (visited on 03/16/2023).

[8] K. Deb et al. "A fast and elitist multiobjective genetic algorithm: NSGA-II". In: *IEEE Transactions on Evolutionary Computation* 6.2 (Apr. 2002). Conference Name: IEEE Transactions on Evolutionary Computation, pp. 182–197. ISSN: 1941-0026. DOI: 10.1109/4235.996017.

[9] Department of the Environment, Climate and Communications. *Climate Action Plan 2023*. May 30, 2023. URL: https://www.gov.ie/pdf/?file=https://assets.gov.ie/256997/b5da0446-8d81-4fb5-991e-65dd807bb257.pdf#page=null (visited on 06/01/2023).

[10] Department of the Environment, Climate and Communications. *National Energy & Climate Plan 2021-2030*. Sept. 14, 2021. URL: https://www.gov.ie/pdf/?file=https://assets.gov.ie/94442/f3e50986-9fde-4d34-aa35-319af3bfac0c.pdf#page=null (visited on 06/01/2023).

[11] D. Diakoulaki, G. Mavrotas, and L. Papayannakis. "Determining objective weights in multiple criteria problems: The critic method". In: *Computers & Operations Research* 22.7 (Aug. 1, 1995), pp. 763–770. ISSN: 0305-0548. DOI: 10.1016/0305-0548(94)00059-H. URL: https://www.sciencedirect.com/science/article/pii/030505489400059H (visited on 04/11/2023).

[12] Quang Vu Dinh et al. "A geospatial method for estimating the levelised cost of hydrogen production from offshore wind". In: *International Journal of Hydrogen Energy* (Jan. 21, 2023). ISSN: 0360-3199. DOI: 10.1016/j.ijhydene.2023.01.016. URL: https://www.sciencedirect.com/science/article/pii/S0360319923000174 (visited on 02/24/2023).

[13] Van Nguyen Dinh et al. "Development of a viability assessment model for hydrogen production from dedicated offshore wind farms". In: *International Journal of Hydrogen Energy*. Recent Trends in Hydrogen Production and Utilization 46.48 (July 13, 2021), pp. 24620–24631. ISSN: 0360-3199. DOI: 10.1016/j.ijhydene.2020.04.232. URL: https://www.sciencedirect.com/science/article/pii/S0360319920316438 (visited on 02/24/2023).

[14] Dmitri Bessarabov, Haijiang Wang, Hui Li, Nana Zhao. *PEM Electrolysis for Hydrogen Production: Principles and Applications*. Routledge & CRC Press. 2016. URL: https://www.routledge.com/PEM-Electrolysis-for-Hydrogen-Production-Principles-and-Applications/Bessarabov-Wang-Li-Zhao/p/book/9781138775497 (visited on 10/18/2022).

[15] European Commission. *REPowerEU: affordable, secure and sustainable energy for Europe*. May 18, 2022. URL: https://commission.europa.eu/strategy-and-policy/priorities-2019-2024/european-green-deal/repowereu-affordable-secure-and-sustainable-energy-europe_en (visited on 06/01/2023).

[16] European Council. *Fit for 55*. May 26, 2023. URL: https://www.consilium.europa.eu/en/policies/green-deal/fit-for-55-the-eu-plan-for-a-green-transition/ (visited on 06/01/2023).

[17] Eurostat. *Share of energy from renewable sources*. Apr. 4, 2023. URL: https://ec.europa.eu/eurostat/databrowser/view/NRG_IND_REN/default/table?lang=en (visited on 06/01/2023).

[18] Petronilla Fragiacomo and Matteo Genovese. "Modeling and energy demand analysis of a scalable green hydrogen production system". In: *International Journal of Hydrogen Energy* 44.57 (Nov. 15, 2019), pp. 30237–30255. ISSN: 0360-3199. DOI: 10.1016/j.ijhydene.2019.09.186. URL: https://www.sciencedirect.com/science/article/pii/S0360319919336341 (visited on 10/18/2022).

[19] Hadi Mosadeghi, Quang Vu Dinh, Paul Leahy. "Efficiency, Commercial Maturity, and Footprint of Subsystems and for Wind-to-Hydrogen Conversion Systems". Unpublished. Unpublished.

[20] Omar S. Ibrahim et al. "Dedicated large-scale floating offshore wind to hydrogen: Assessing design variables in proposed typologies". In: *Renewable and Sustainable Energy Reviews* 160 (May 1, 2022), p. 112310. ISSN: 1364-0321. DOI: 10.1016/j.rser.2022.112310. URL: https://www.sciencedirect.com/science/article/pii/S1364032122002258 (visited on 03/16/2023).

[21] IEA. *Global Hydrogen Review 2022*. 2022, p. 284. URL: https://iea.blob.core.windows.net/assets/c5bc75b1-9e4d-460d-9056-6e8e626a11c4/GlobalHydrogenReview2022.pdf (visited on 05/31/2023).

[22] IRENA. *FUTURE OF WIND - Deployment, investment, technology, grid integration and socio-economic aspects*. Oct. 2019. URL: https://www.irena.org/-/media/Files/IRENA/Agency/Publication/2019/Oct/IRENA_Future_of_wind_2019.pdf?rev=c324896ba0f74c99a0cde784f3a36dff.

[23] IRENA. *Green hydrogen for industry: A guide to policy making*. 2022. URL: https://www.irena.org/-/media/Files/IRENA/Agency/Publication/2022/Mar/IRENA_Green_Hydrogen_Industry_2022_.pdf?rev=720f138dbfc44e30a222

[24] IRENA. *Hydrogen from renewable power: Technology outlook for the energy transition*. Sept. 6, 2018. URL: https://www.irena.org/publications/2018/Sep/Hydrogen-from-renewable-power (visited on 03/20/2023).

[25] IRENA. *Renewable Energy Statistics 2022*. 2022. URL: https://www.irena.org/publications/2022/Jul/Renewable-Energy-Statistics-2022.

[26] A. Kafetzis et al. "Energy management strategies based on hybrid automata for islanded microgrids with renewable sources, batteries and hydrogen". In: *Renewable and Sustainable Energy Reviews* 134 (Dec. 1, 2020), p. 110118. ISSN: 1364-0321. DOI: 10.1016/j.rser.2020.110118. URL: https://www.sciencedirect.com/science/article/pii/S1364032120304093 (visited on 03/16/2023).

[27] Joseph J. Kelly and Paul G. Leahy. "Sizing Battery Energy Storage Systems: Using Multi-Objective Optimization to Overcome the Investment Scale Problem of Annual Worth". In: *IEEE Transactions on Sustainable Energy* 11.4 (Oct. 2020), pp. 2305–2314. ISSN: 1949-3029, 1949-3037. DOI: 10.1109/TSTE.2019.2954673. URL: https://ieeexplore.ieee.org/document/8907493/ (visited on 01/23/2023).

[28] Marius C. Möller and Stefan Krauter. "Hybrid Energy System Model in Matlab/Simulink Based on Solar Energy, Lithium-Ion Battery and Hydrogen". In: *Energies* 15.6 (Jan. 2022). Number: 6 Publisher: Multidisciplinary Digital Publishing Institute, p. 2201. ISSN: 1996-1073. DOI: 10.3390/en15062201. URL: https://www.mdpi.com/1996-1073/15/6/2201 (visited on 10/18/2022).

[29] Musial, Walter, Philipp Beiter, Jake Nunemaker, Donna Heimiller, Josh Ahmann, and Jason Busch. *Oregon Offshore Wind Site Feasibility and Cost Study*. 2019. URL: https://www.nrel.gov/docs/fy20osti/74597.pdf. (visited on 03/08/2023).

[30] V. Papadopoulos et al. "Improving the utilization factor of a PEM electrolyzer powered by a 15ăMW PV park by combining wind power and battery storage Feasibility study". In: *International Journal of Hydrogen Energy* 43.34 (Aug. 23, 2018), pp. 16468–16478. ISSN: 0360-3199. DOI: 10.1016/j.ijhydene.2018.07.069. URL: https://www.sciencedirect.com/science/article/pii/S0360319918322171 (visited on 10/18/2022).

[31] Philipp Lettenmeier. *Efficiency Electrolysis, White paper*. 2021. URL: https://assets.siemens-energy.com/siemens/assets/api/uuid:a33a8c39-b694-4d91-a0b5-4d8c9464e96c/efficiency-white-paper.pdf (visited on 03/14/2023).

[32] *Renewables.ninja*. URL: https://www.renewables.ninja/ (visited on 02/27/2023).

[33] Fabian Scheepers et al. "Temperature optimization for improving polymer electrolyte membrane-water electrolysis system efficiency". In: *Applied Energy* 283 (Feb. 1, 2021), p. 116270. ISSN: 0306-2619. DOI: 10.1016/j.apenergy.2020.116270. URL: https://www.sciencedirect.com/science/article/pii/S0306261920316603 (visited on 03/14/2023).

[34] Sustainable Energy Authority of Ireland (SEAI). *ENERGY IN IRELAND 2022 Report*. Dec. 2022. URL: https://www.seai.ie/publications/Energy-in-Ireland-2022.pdf (visited on 05/30/2023).

[35] Sustainable Energy Authority of Ireland (SEAI). *Renewable Energy in Ireland*. Sustainable Energy Authority Of Ireland. URL: https://www.seai.ie/data-and-insights/seai-statistics/key-statistics/renewables/index.xml (visited on 06/01/2023).

[36] Hammou Tebibel. "Methodology for multi-objective optimization of wind turbine/battery/electrolyzer system for decentralized clean hydrogen production using an adapted power management strategy for low wind speed conditions". In: *Energy Conversion and Management* 238 (June 15, 2021), p. 114125. ISSN: 0196-8904. DOI: 10.1016/j.enconman.2021.114125. URL: https://www.sciencedirect.com/science/article/pii/S0196890421003010 (visited on 10/18/2022).

[37] Hammou Tebibel and Sifeddine Labed. "Design and sizing of stand-alone photovoltaic hydrogen system for HCNG production". In: *International Journal of Hydrogen Energy* 39.8 (Mar. 6, 2014), pp. 3625–3636. ISSN: 0360-3199. DOI: 10.1016/j.ijhydene.2013.12.124. URL: https://www.sciencedirect.com/science/article/pii/S0360319913031169 (visited on 03/13/2023).

[38] Øystein Ulleberg. "The importance of control strategies in PVhydrogen systems". In: *Solar Energy*. Solar World Congress 2001 76.1 (Jan. 1, 2004), pp. 323–329. ISSN: 0038-092X. DOI: 10.1016/j.solener.2003.09.013. URL: https://www.sciencedirect.com/science/article/pii/S0038092X03003554 (visited on 10/18/2022).

[39] Vilayanur Viswanathan et al. *2022 Grid Energy Storage Technology Cost and Performance Assessment*. 2022. URL: https://www.pnnl.gov/sites/default/files/media/file/ESGC%20Cost%20Performance%20Report%202022%20PNNL-33283.pdf.

[40] Lukas Weimann et al. "Optimal hydrogen production in a wind-dominated zero-emission energy system". In: *Advances in Applied Energy* 3 (Aug. 25, 2021), p. 100032. ISSN: 2666-7924. DOI: 10.1016/j.adapen.2021.100032. URL: https://www.sciencedirect.com/science/article/pii/S2666792421000251 (visited on 03/16/2023).

[41] Chuanbo Xu et al. "Data-driven configuration optimization of an off-grid wind/PV/hydrogen system based on modified NSGA-II and CRITIC-TOPSIS". In: *Energy Conversion and Management* 215 (July 1, 2020), p. 112892. ISSN: 0196-8904. DOI: 10.1016/j.enconman.2020.112892. URL: https://www.sciencedirect.com/science/article/pii/S0196890420304301 (visited on 10/20/2022).

[42] Tevfik Yigit and Omer Faruk Selamet. "Mathematical modeling and dynamic Simulink simulation of high-pressure PEM electrolyzer system". In: *International Journal of Hydrogen Energy* 41.32 (Aug. 24, 2016), pp. 13901–13914. ISSN: 0360-3199. DOI: 10.1016/j.ijhydene.2016.06.022. URL: https://www.sciencedirect.com/science/article/pii/S0360319916318341 (visited on 03/13/2023).

[43] Behnam Zakeri and Sanna Syri. "Electrical energy storage systems: A comparative life cycle cost analysis". In: *Renewable and Sustainable Energy Reviews* 42 (Feb. 1, 2015), pp. 569–596. ISSN: 1364-0321. DOI: 10.1016/j.rser.2014.10.011. URL: https://www.sciencedirect.com/science/article/pii/S1364032114008284 (visited on 02/03/2023).

Acknowledgments

This thesis represents the culmination of a long journey, filled with challenges and difficult moments, but also moments of satisfaction and joy, began during the pandemic and concluded with an incredible international experience.

First and foremost, I would like to express my gratitude to the individuals who made the writing of this manuscript possible. I extend my sincere thanks to my supervisor, Professor Anna Stoppato, for her precious help and availability. I am deeply grateful to the entire H-Wind team, who welcomed me and made me feel part of the group. In particular, I want to thank Professor Paul Leahy for his continuous support and kindness, which gave me more confidence in my work during those moments where it seemed there wasn't any possible solution. Also, a special thank you goes to Quang Vu Dinh and Hadi Mosadeghi for all their advice and suggestions, which made this project easier to carry on.

My master's degree did not start in the enthusiastic way I was foreseeing for the final part of my studies, heavily affected by the lockdown due to the pandemic, which turned the usual university life into a disconnected way of following online lectures, without any contact with fellow learners. But I feel deeply grateful to the student association of Padova *LEDS - L'Energia Degli Studenti* that completely transformed this study experience, giving me the opportunity to reconnect with people during a challenging period, establishing meaningful friendships, as well as reigniting my enthusiasm for learning and curiosity in new energy topics, making me desire to deepen my knowledge.
I would also like to thank some friends, that expecially during my last semester in Padova absolutely improved my experience as a student, having fun and sharing meaningful moment with them: thank you Elisabetta, Matteo, Davide, Laura, Luca, Annachiara, Mathea, Synne, Inga, Cecilie and Janik.

This study journey couldn't finish in a better way, with almost a year in that stunning country that is Ireland. Many are the people I met and shared talks, laughs and Beamish pints with, and I feel so privileged that our paths crossed. Among them I want to thank all the *Graffiti People*, Mayank, Alessandro, Cyann, Maïa, Erik, Marie M., Marie B., Robin, Hilde, Francesca, Rin and Yun. An open hearted *danke, merci* and *kiitos* goes in particular to Semira, and the *Tree Gangers* Cécile and Mikko: you have been my dearest friends in such a wonderful fragment of my life, and without you it wouldn't have been the same.
Also, a *go raibh míle míle maith agaibh* to all my Irish class *múinteoirí* Karol Coleman, Nuala de Búrca, Claire Ní Mhuirthile and Seán Ó Laoi, that through their great enthusiasm for that beautiful language, allowed me to experience the irish culture from a closer perspective.

Finally, a special thanks to all my friends here, Enrico, Alberto Z., Ilaria, Luca, Erica, Elena, Nicolò, Petra, Alberto M., Irene, Filippo and Simone, for all the great time with had together and your support throughout all this time.

Last, but absolutely not least, a huge *grazie di cuore* to my family and my nephews. This would not have been possible without your support and your help, and I will be always grateful for that. I love you all.